Allele-specific endogenous tagging and quantitative analysis of β-catenin in colon cancer cells

Giulia Ambrosi[1], Oksana Voloshanenko[1], Antonia F. Eckert[2], Dominique Kranz[1], G. Ulrich Nienhaus[2,3,4,5], Michael Boutros[1,*]

[1]German Cancer Research Center (DKFZ), Division of Signaling and Functional Genomics and Heidelberg University, BioQuant and Medical Faculty Mannheim, D-69120 Heidelberg, Germany
[2]Institute of Applied Physics, Karlsruhe Institute of Technology, D-76049 Karlsruhe, Germany
[3]Institute of Nanotechnology, Karlsruhe Institute of Technology, D-76021 Karlsruhe, Germany
[4]Institute of Biological and Chemical Systems, Karlsruhe Institute of Technology, D-76021 Karlsruhe, Germany
[5]Department of Physics, University of Illinois at Urbana-Champaign, Urbana, IL 61801, USA

*Address for correspondence: m.boutros@dkfz.de, Fax: +49 6221 421959

ABSTRACT

Wnt signaling plays important roles in embryonic development and during tissue homeostasis, and its deregulation contributes to the onset and progression of tumors. β-catenin is a key component of the 'canonical' Wnt pathway. Upon activation of the pathway, β-catenin is stabilized and enters the nucleus to bind transcription factors and activate Wnt target genes. Mutations that activate β-catenin have been found in many gastrointestinal tumors, including colorectal and hepatocellular carcinomas. However, the dynamics of wild-type and mutant forms of β-catenin are not fully understood. Here, we engineered fluorescently tagged alleles of the endogenous β-catenin by CRISPR/Cas9 in a colorectal cancer cell line. We generated a cell model which carries wild-type and the oncogenic **Δ**45 mutant allele tagged with different fluorescent proteins, enabling the functional and biochemical analysis of both variants in the same cell. Endogenously tagged β-catenin remains functional, responds to Wnt pathway activation and does not interfere with the role of β-catenin in cell-cell adhesion. We then analyzed their biochemical and biophysical properties using immunoprecipitation, immunofluorescence and fluorescence correlation spectroscopy approaches. Our results show that wild-type and mutant β-catenin have distinct biophysical properties. In addition, activation of Wnt signaling by treatment with a GSK3β inhibitor or truncating *APC* mutation modulated the wild-type allele to mimic the properties of the mutant β-catenin allele found in colorectal cancer. The one-step tagging strategy also demonstrates how CRISPR/Cas9-mediated genome engineering can be employed for the concurrent functional analysis of wild-type and mutant alleles.

Keywords: Wnt signaling; β-catenin; *CTNNB1*; endogenous tagging; CRISPR; fluorescence correlation spectroscopy; FCS; oncogenic signaling; cancer

INTRODUCTION

Wnt signaling plays fundamental roles in many biological processes in development, stem cell maintenance and disease (Clevers and Nusse, 2012; Zhan et al., 2017). A key regulator of 'canonical' Wnt signaling is β-catenin (*CTNNB1*). When Wnt signaling is inactive, β-catenin forms part of the destruction complex, which consists of adenomatous polyposis coli (APC), axis inhibition protein 1 (Axin1) (Li et al., 2012), casein kinase 1α (CK1α) and glycogen synthase kinase 3β (GSK3β). In the destruction complex, β-catenin is N-terminally phosphorylated by CK1 kinase at Ser45 (Hagen and Vidal-Puig, 2002) and then sequentially phosphorylated by GSK3β at residues Ser33, Ser37 andThr41 (Liu et al., 2002). Subsequently, phospho-β-catenin is targeted for proteasomal degradation by the $SCF^{ßTrCP}$ E3-ligase complex (Wu et al., 2003).

Wnt signaling is activated when Wnt ligands bind to seven-pass transmembrane receptors of the Frizzled (Fzd) protein family and the transmembrane LRP5/6 (low-density lipoprotein receptor-related protein) co-receptor (Bilic et al., 2007; Cong et al., 2004). Fzd proteins then recruit the cytosolic adaptor protein Dishevelled (Dvl) to the cell membrane *via* its DEP domain, leading to polymerization of Dvl (Schwarz-Romond et al., 2007). Dvl facilitates membrane recruitment of Axin1 by a DIX-DIX domain heterotypic interaction (Cliffe et al., 2003), which in turn stimulates GSK3β- and CK1α- mediated phosphorylation of the LRP5/6 cytosolic tail in its five PPPSPxS motifs and its binding to LRP5/6 (Stamos et al., 2014). As a consequence, the destruction complex disassembles, β-catenin is no longer degraded and translocates into the nucleus. In the nucleus, β-catenin interacts with T cell factor (TCF)/lymphoid enhancer binding factor (LEF) family of transcription factors and activates target genes in a cell-type dependent manner. In addition to its role in Wnt signaling, β-catenin is also found at cell-cell adherens junctions (AJs) mediating the interactions between the cytoplasmic domain of cadherins and the actin cytoskeleton (Aberle et al., 1994; Hoschuetzky et al., 1994; Huber and Weis, 2001).

The human β-catenin protein consists of 781 amino acids and contains three distinct structural domains. Crystal structure and NMR analysis of β-catenin reveal that both N- and C-terminal domains are structurally flexible, whereas the central armadillo repeat has a rather rigid scaffold structure (Huber et al., 1997; Orsulic and Peifer, 1996; Xing et al., 2008). The N-terminus is crucial for its stability and for cell adhesion by interacting with α-catenin. This region also contains evolutionarily conserved serine and tyrosine residues that are phosphorylated by CK1α- and GSK3β, which facilitate protein ubiquitination and proteasomal degradation (Valenta et al., 2012). Deregulation of Wnt signaling components is associated with a variety of human diseases, ranging from growth-related pathologies to cancer (Clevers and Nusse, 2012; Zhan et al., 2017),

however, overactive Wnt signaling has been difficult to target (Zhong and Virshup, 2020). Mutations in *CTNNB1*/β-catenin in colorectal cancer are found in its N-terminal domain, particularly in exon 3 that carries multiple phosphorylation sites for CK1 and GSK3β including Ser33/Ser37/Thr41/Ser45 (Cancer Genome Atlas Network, 2012; Dar et al., 2017; Jamieson et al., 2011). Mutations or deletion of these sites, often in only one allele, prevent phosphorylation of β-catenin, which results in its accumulation and subsequent activation of Wnt pathway target genes. However, the biochemical and biophysical properties of different β-catenin alleles in their endogenous loci have remained largely unknown.

To functionally analyze proteins, the introduction of small immune epitopes or fluorescent tags in-frame of the genomic locus enables their visualization and quantitative analysis. Here, we aimed to study the behaviour of wild-type and a mutant oncogenic β-catenin. We made use of the colon cancer cell line HCT116 which harbors one wild-type and one mutant ∆Ser45 β-catenin allele to generate endogenously tagged β-catenin by CRISPR/Cas9 genome editing. We engineered a HCT116 clone with mClover-tagged wild-type β-catenin and mCherry-tagged mutant β-catenin. Tagging wild-type and mutant β-catenin in the same cell provided an opportunity to compare the function and behaviour of both proteins simultaneously. Our results indicate that wild-type and mutant β-catenin exist in two separate pools differing in their physical properties. Moreover, treatment with a GSK3β inhibitor or introduction of a truncating mutation of *APC* changed the physical properties of wild-type β-catenin, phenocopying the ∆Ser45 mutant form.

RESULTS

Strategy to generate endogenously tagged fluorescent β-catenin isoforms

Previously, the dynamics and biochemical properties of β-catenin in cells were investigated by using transiently or stably expressed GFP/YFP-fusion proteins (Giannini et al., 2000; Jamieson et al., 2011; Kafri et al., 2016; Krieghoff et al., 2006). To study wild-type and mutant β-catenin on a physiological level, we utilized the diploid colon cancer cell line HCT116 that harbors both a wild-type and a ∆Ser45 mutant allele. This in-frame ∆Ser45 deletion results in a loss of phosphorylation at this position, leading to the stabilization of β-catenin and constant activation of Wnt downstream targets (Hagen and Vidal-Puig, 2002).

To generate endogenously tagged β-catenin, we applied a gene replacement strategy using CRISPR/Cas9 editing (Mali et al., 2013; Ran et al., 2013; Yang et al., 2014) to introduce different fluorescent tags in the two alleles of the β-catenin locus of HCT116 cells in one-step

(Figure 1, S1A). To this end, we identified a suitable sgRNA sequence 5'-TGACCTGTAAATCATCCTTTAGG-3' (Heigwer et al., 2014) for targeting the C-terminal region of β-catenin. This target site was chosen because it has previously been shown that C-terminal tagging did not affect its function in overexpression experiments (Giannini et al., 2000; Jamieson et al., 2011; Kafri et al., 2016; Krieghoff et al., 2006). Then, two donor templates with 180bp homology arms were designed close to the sgRNA PAM sequence (Elliott et al., 1998; Natsume et al., 2016) and with two different fluorophores. Here we chose mClover3 and mCherry2 for their favorable biophysical properties such as spectral absorbance, brightness, photostability and maturation time (Lam et al., 2012; Shaner et al., 2004; Thorn, 2017). In the following, for the sake of brevity, we will refer to these two fluorescent proteins as Clover and Cherry, respectively. Moreover, FLAG and V5-tags were integrated in front of the fluorescent proteins to enable a broad spectrum of downstream applications. To avoid steric hindrance of the different domains, a flexible GS linker consisting of three repeats of glycine and serine residues (Gly-Gly-Gly-Gly-Ser)n was inserted between the C-terminal domain of β-catenin (Trinh et al., 2004) (Figure 1, S1A). Gene resistance cassettes flanked by loxP sites were also introduced after the fluorescent proteins for selection of edited cells after homology-directed repair (HDR) (Smirnikhina et al., 2019). Selection cassettes encoded for the antibiotic resistance hygromycin and blasticidin, and for the Clover and Cherry donor template, respectively (Figure S1A). The loxP sites were included to allow cassette removal upon Cre-mediated gene disruption recombinase technology.

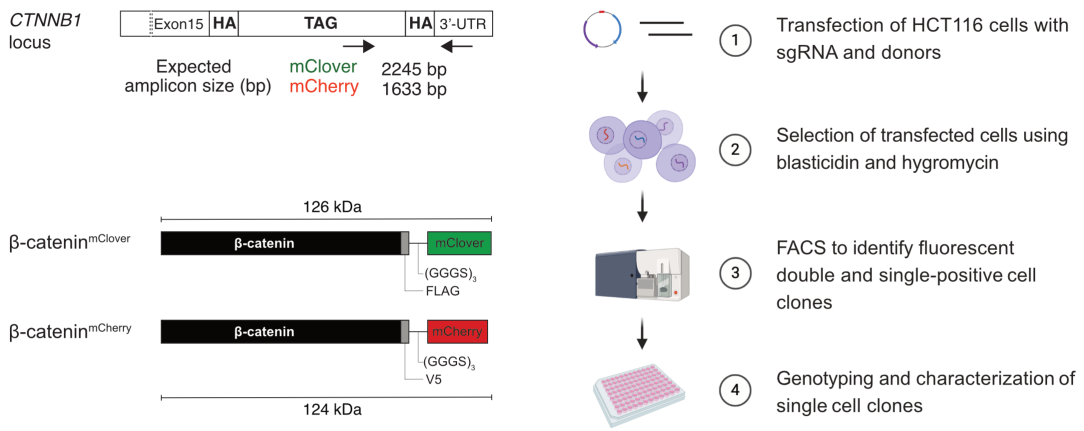

Figure 1: Strategy and workflow for bi-allelic fluorescent tagging of β-catenin in colon cancer cells. (Left panels) Schematic representation of *CTNNB1*/β-catenin tagging strategy, the CTNNB1/β-catenin locus and tagged β-catenin proteins. (Right panels) Workflow for the generation of endogenously tagged β-catenin in HCT116 colorectal cancer cells. See also Figure S1A for more details. HA: homology arm; UTR; untranslated region.

Generation and characterization of β-catenin tagged cells

To generate cell lines with endogenously allele-specific tagged β-catenin, we transfected HCT116 cells with plasmids encoding for both the sgRNA targeting β-catenin (sgCTNNB1) and Cas9 protein from *S. pyrogenes* (Mali et al., 2013) and the donor template encoding either V5-mCherry BRS (blasticidinS) or FLAG-mClover HygR (hygromycin resistance) (Figure 1, S1A). Transfected HCT116 cells were first selected with puromycin for 48 h and subsequently with blasticidin/hygromycin for five days. Pooled edited cells were analyzed and sorted into single cell clones by fluorescence-activated cell sorting (FACS) (Figure 1, S1B). Low fluorophore expression was observed, regardless whether a single donor template was used (1.4% of Cherry- and 17.3% of Clover-labeled cells) or both donors were co-transfected simultaneously (0.9% of only Cherry-, 7.4% of only Clover- and 0.1% of double-labelled cells) (Figure S1B).

In total, 44 single cell clones were sorted by FACS and expanded for further characterization which included double-positive and single-positive cells. To identify correctly edited clones, genotyping was performed using a set of primer pairs (Figure S2A). Primer pair (a) was designed to bind to the β-catenin genomic locus flanking the donor cassettes. Clone #37 showed the expected higher molecular weight bands indicating that both alleles of the *CTNNB1* were correctly edited. By contrast, clones #33, #45 and #24 showed two amplicons using primer pair (a). The lower band represents the wild-type, as observed in parental (β-catenin$^{wt/\Delta 45}$) and β-catenin$^{wt/-}$ cell lines, and the higher band represents the fluorophore-edited genomic locus. In addition, PCRs were performed using primer pairs (b) and (b') which detect the integration of Cherry- or Clover-tags, respectively. As shown in Figure S2A, clones #33, #37 and #24 displayed the expected amplicon with the Clover specific primers (b'), whereas only clones #37 and #45 had the expected amplicon with the Cherry specific primers (b). Furthermore, we used primer pair (c) binding to the homologous region of both donor cassettes and primer pair (d) binding inside the fluorescent tag. For all four clonal #33, #37, #45 and #24 cell lines, the expected bands were detected indicating correct editing (Figure S2A). In agreement to the first PCRs, clone #37 showed two bands representing correct integration of both, Clover and Cherry. As expected from the initial experiments, clones #33 and #24 showed the right molecular weight band representing Clover, whereas clone #45 showed only the lower amplicon representing Cherry. In summary, from the 44 analyzed single cell lines, only a single cell line (clone #37) showed the correct insertion of both fluorophores in the *CTNNB1* locus (Figure S2B). In addition, seven clones showed a heterozygous integration of Cherry fluorophore in the β-catenin locus and 24 clones were heterozygous for the Clover-tagged allele fluorophore. Six clones harbored an insertion in the

CTNNB1 wild-type allele presumably due to non-homologous end joining (NHEJ). Two isogenic cell lines had partial integration of the Clover tag and four clones were wild type indicating no editing events in the *CTNNB1* locus (Figure S2B).

To confirm the editing events, genomic DNA, mRNA and protein lysates were analyzed and compared to the parental HCT116 (β-catenin$^{wt/\Delta 45}$) cell line and to an HCT116 isogenic cell line in which the ΔSer45 allele was removed (β-catenin$^{wt+/-}$) (Chan et al., 2002). Sanger sequencing of PCR amplicons of the target site revealed correct in-frame integration of fluorophores confirming that clone #37 harbors Clover- and Cherry tagged β-catenin. In accordance with the genotyping results, clones #24, #33, #45 were found to be heterozygous with one remaining WT allele. Subsequently, PCR was performed to determine tagging of alleles (WT and ΔSer45) using cDNA from reverse-transcribed mRNA of each isogenic cell line. Sanger sequencing of cDNA templates revealed that both clones #37 and #45 carried the Cherry fluorophore in the ΔSer45 allele (Figure 2A). In contrast, #33 and #37 clones harbored the Clover fluorophore in the wild-type allele, as indicated by the in-frame sequence with Ser45.

Next, total cell lysates of parental and isogenic knock-in cell lines were analyzed for β-catenin fusion proteins by western blot. As shown in Figure 2B, clone #33 and clone #45 have wild-type β-catenin (94kDa) and the additional tagged variants of β-catenin, whereas clone #37 has two high molecular weight bands indicative of both tagged β-catenin variants. Furthermore, immunoprecipitations using either affinity beads for the Clover (GFP) and Cherry fluorophores, or anti-β-catenin antibodies were performed and analyzed by western blotting. As shown in Figure 2C, in GFP-immunoprecipitated lysates of clone #37 a β-catenin variant at around 126kDa was detected that was also recognized by GFP and β-catenin antibodies. By contrast, β-catenin immunopurified lysates revealed two different bands at around 120 kDa that were also recognized by β-catenin, V5 and Cherry antibodies. Pulldown with a β-catenin antibody demonstrated two different β-catenin variants that were either detected by GFP or Cherry/V5 antibodies. Thus, these results confirm the presence of two differently tagged β-catenin variants in clone #37 at the protein level. Similarly, we analyzed clones #33 and clone #45 by immunoprecipitation (Figure S2C). In clone #33, GFP-immunoprecipitated lysates showed a β-catenin variant at around 126 kDa that was also present upon immunoprecipitation with the β-catenin antibody. Here, wild-type β-catenin (94kDa) was pulled down in addition to the β-catenin variant (Figure S2C). By contrast, Cherry-immunoprecipitation identified two bands of around 120 kDa in clone #45 that were also recognized by β-catenin, Cherry and V5 antibodies. Pulldown with a β-catenin antibody showed the two high molecular weight bands that were recognized by the Cherry antibody, whereas the band at 94kDa was only recognized by the β-catenin antibody.

In summary, these experiments confirmed the bi-allelic endogenous tagging of two alleles of β-catenin with different fluorophores, thereby enabling the analysis of wild-type and mutant forms of β-catenin in the same cell.

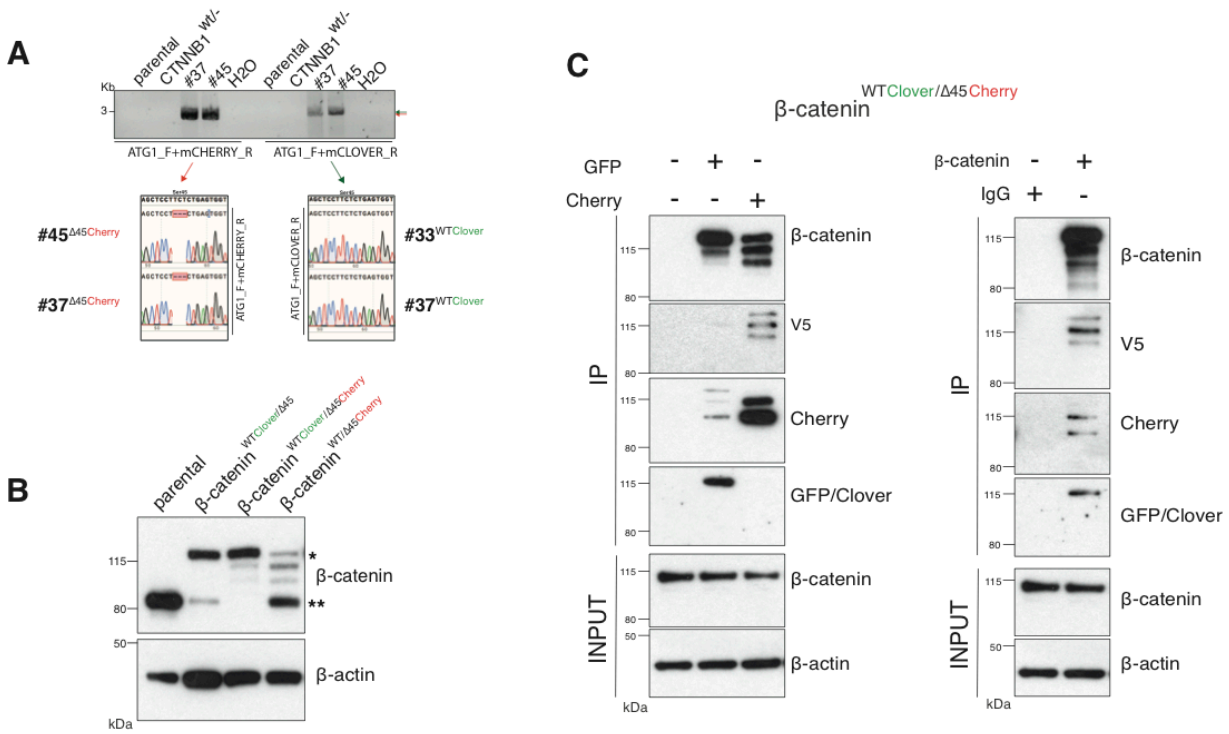

Figure 2: Identification and confirmation of tagged β-catenin alleles. (A) Sanger sequencing confirms bi-allelic tagging of β-catenin. Sequencing results show clones #45 (β-catenin$^{wt/\Delta45Cherry}$) and #37 (β-catenin$^{wtClover/\Delta45Cherry}$) Cherry is in-frame with the mutant allele and clones #33 (β-catenin$^{wtClover/\Delta45}$) and #37 (β-catenin$^{wtClover/\Delta45Cherry}$) Clover is in-frame with wild-type allele (codon TCT). (B) Cell lysates of indicated HCT116 cell lines analysed by western blotting with a β-catenin antibody; β-actin served as a loading control. *tagged, **wild-type β-catenin. (C) HCT116 β-catenin$^{wtClover/\Delta45Cherry}$ (clone #37) immunoprecipitation with GFP, Cherry and control beads or with a β-catenin antibody followed by immunoblotting with indicated antibodies. Representative results from three independent experiments are shown. kDa: kilo Dalton.

Functional characterization of endogenously tagged β-catenin cell lines

To test whether the C-terminal fluorescence tags of β-catenin interfere with its physiological functions, we tested these novel cell lines in different assays. First, we compared cell proliferation of the clonal cell lines to the parental β-catenin$^{wt/\Delta45}$ and the β-catenin$^{wt+/-}$ cell line, which only had a wild-type but not a mutant β-catenin allele. All three clones #33, #37 and #45 showed a similar growth behaviour as the parental β-catenin$^{wt/\Delta45}$ cells (Figure 3A), whereas the cell line carrying only one wild-type allele (β-catenin$^{wt+/-}$) displayed an impaired growth.

Next, we tested the functionality and localization of the endogenously tagged β-catenin variants. We performed siRNA-mediated silencing of β-catenin and analysed gene expression by RT-qPCR (Figure 3B, Figure S3A), which showed that downregulation of β-catenin led to the reduction in fluorophore levels as well as the Wnt target gene *AXIN2.* Consistently, depletion of β-catenin showed a reduction of Cherry and Clover by immunofluorescence on the protein level (Figure 3C, Figure S3A).

In addition to its role in Wnt signaling, β-catenin interacts with the cytoplasmic domains of E-cadherin and α-catenin to bridge the cell-adhesion complex and actin cytoskeleton inside the cells, thereby localising it to the cell membrane (Aberle et al., 1994; Hoschuetzky et al., 1994). Immunofluorescence analysis confirmed the localization of the endogenously tagged β-catenin variants at the cell membrane as observed in the parental HCT116 cell line (Figure 3D, Figure S3B). Immunoprecipitation with an E-cadherin antibody demonstrated the interaction of β-catenin and E-cadherin in all clones (Figure 3E, Figure S3C). Interestingly, wild-type β-catenin appeared to have a higher binding affinity for E-cadherin than the mutant form, as shown in clones #33 and #45 (Figure S3C).

Taken together, these results indicate that endogenously Cherry- and Clover-tagged β-catenin proteins do not behave differently from the untagged β-catenin variants regarding localization, cell-cell adhesion and Wnt pathway activity.

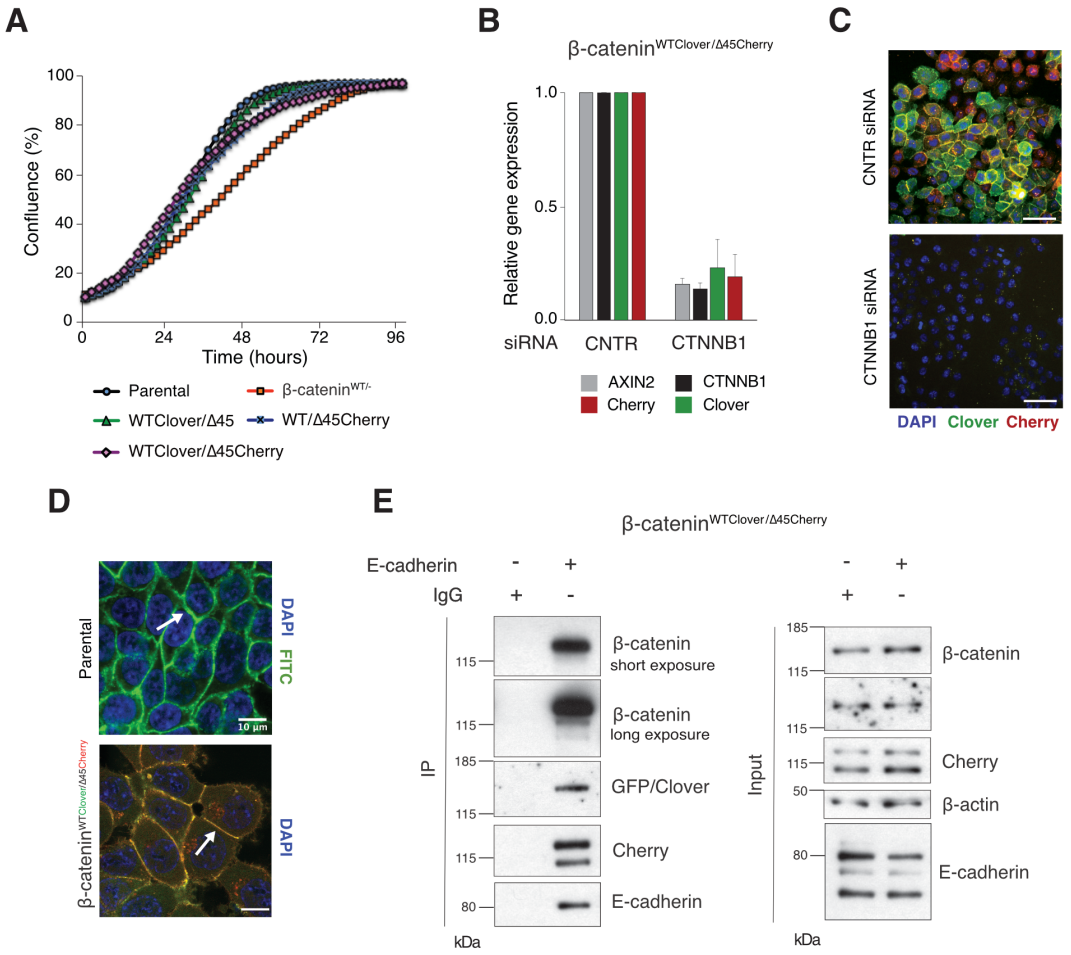

Figure 3. Fluorescently tagged β-catenin variants are functional and localize to adherens junctions. (A) Proliferation of the indicated HCT116 cell clones was monitored by live-cell imaging using an Incucyte instrument. (B) In HCT116 β-catenin$^{wtClover/\Delta45Cherry}$, mRNA-levels of *CTNNB1*, *AXIN2*, *Cherry* and *Clover* were determined by RT-qPCR in control conditions and upon depletion of *CTNNB1*/β-catenin by siRNA. (C) Representative immunofluorescence images of HCT116 β-catenin$^{wtClover/\Delta45Cherry}$ after siRNA-mediated knockdown of *CTNNB1* is shown (n=3; mean ± SEM; scale bars: 100µm). (D) β-catenin accumulates at cell-cell junctions (arrow). Representative immunofluorescence images of HCT116 β-catenin$^{wtClover/\Delta45Cherry}$ and parental HCT116 β-catenin$^{wt/\Delta45}$ stained with a β-catenin antibody is shown. Scale bars: 10µm. (E) Immunoprecipitation of HCT116 clone β-catenin$^{wtClover/\Delta45Cherry}$ with E-cadherin confirms its interaction with β-catenin. Representative results from three independent experiments are shown. kDa: kiloDalton.

Wild-type and mutant β-catenin variants contribute both to canonical Wnt signaling output

We next investigated the impact of endogenously tagged β-catenin on the activation of Wnt signaling. Wnt activity was measured by TCF4/Wnt-dependent reporter assay and analyzing *AXIN2* levels in the isogenic knock-in clones and parental cell line upon treatment with either the GSK3β inhibitor CHIR99021 or ICG-001, an inhibitor of CBP/β-catenin interaction (Figure 4A). Upon CHIR9991 treatment, TCF4/Wnt-reporter activity was induced and *AXIN2* gene expression levels were increased similarly in all isogenic cell lines. Treatment with the Wnt inhibitor ICG001 decreased Wnt reporter activity and *AXIN2* expression levels in all cell lines, as expected (Figure 4A). In addition, immunofluorescence analysis demonstrated that after addition of CHIR99021, nuclear β-catenin was increased in all clones indicative of increased nuclear translocation of β-catenin upon Wnt activation (Figure 4B, S4). Consistent with its mechanism of action, treatment with ICG001 did neither affect cytoplasmic nor nuclear β-catenin localization in the endogenously tagged or parental cell clones.

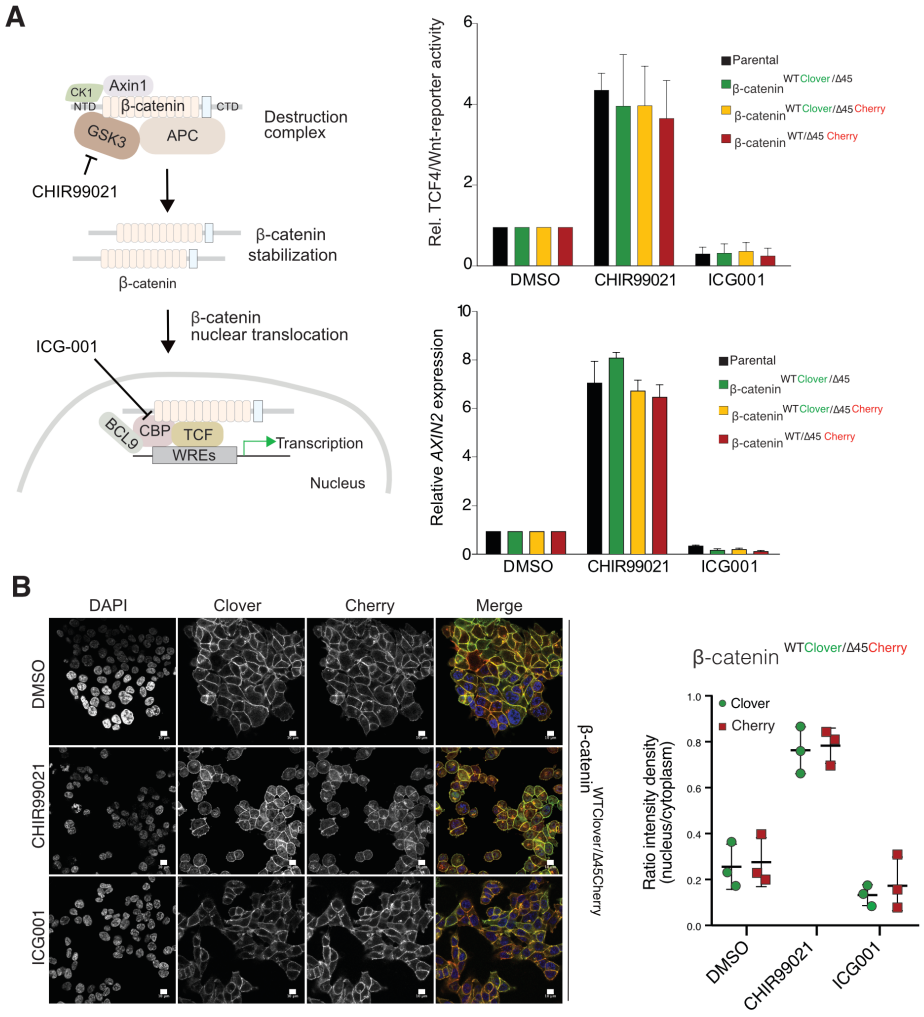

Figure 4. Tagging of β-catenin does not affect functionality in canonical Wnt signalling. (A) Left: Scheme showing the mode of action of GSK3β inhibitor CHIR99021 and CBP inhibitor ICG-001. Right: Indicated HCT116 cell lines were treated with 10μM CHIR99021 and 10μM ICG-001 for 24 hours, then Wnt activity was determined by a luciferase-based TCF4/Wnt-reporter assay (upper panel) and quantification of *AXIN2* mRNA-levels by RT-qPCR (n=3; mean ±SEM). (B) Immunofluorescence analysis HCT116 β-catenin$^{wtClover/\Delta45Cherry}$ after 24 hours treatment with 10μM CHIR99021 and 10μM ICG-001 is shown, scale bar: 10μm. The graph on the right depicts the ratio of nuclear to cytoplasmic fluorescent signal intensity for Clover and Cherry in HCT116 β-catenin$^{wtClover/\Delta45Cherry}$. Data from three independent experiments, each with at least 250 cells per condition, are shown as mean ±SEM. Every experiment includes at least 250 cells per condition. Scale bar: 10μm. WRE: Wnt responsive element.

To analyze the impact of both wild-type and mutant variants on Wnt signaling, we performed knock-down experiments with siRNAs targeting either Cherry or Clover, thereby depleting either mutant or wild-type β-catenin alleles. Silencing of either Clover or Cherry in clone #37 reduced β-catenin and *AXIN2* expression levels in a similar manner, whereas combined knockdown of both had an additive effect comparable to siRNA β-catenin/*CTNNB1* (Figure 5A). Interestingly, silencing of wild-type β-catenin using a siRNA (GFP) resulted in a two-fold increase

of mutant Cherry-tagged β-catenin that was also observed by increased immunofluorescence staining, suggesting a regulatory feedback mechanism (Figure 5B). These results indicate that both wild-type and mutant β-catenin alleles contribute to Wnt activity. This is also consistent with previous results in HCT116 cells demonstrating that Wnt secretion is essential for maintaining Wnt activity (Voloshanenko et al., 2013).

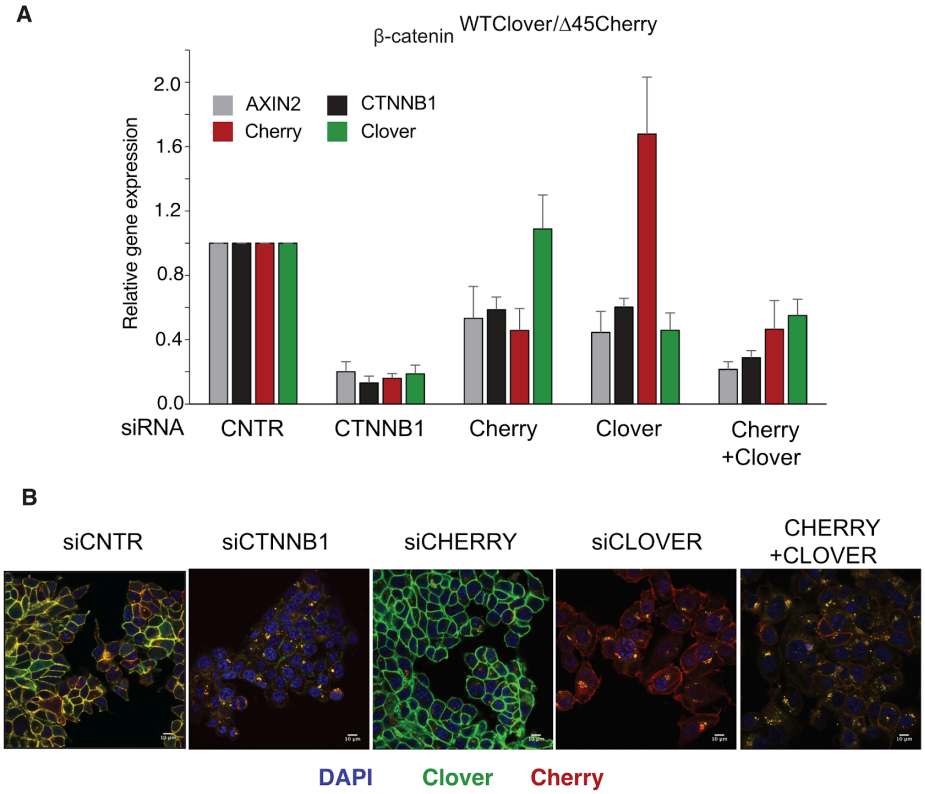

Figure 5. Wild-type and mutant β-catenin both contribute to Wnt pathway activation. (A) Expression levels of *AXIN2*, *CTNNB1*/β-catenin, *Cherry* and *Clover* were measured 72 hours after knockdown with siRNAs directed against Clover, Cherry or both in HCT116 β-catenin$^{wtClover/\Delta45Cherry}$ (n=3, mean ±SEM). (B) Immunofluorescence analysis of HCT116 β-catenin$^{wtClover/\Delta45Cherry}$ upon transfection with siRNAs targeting CTNNB1, Clover, Cherry or a combination of Clover and Cherry. Scale bar: 10µm.

Fluorescence correlation spectroscopy (FCS) reveals differences in the dynamics of wild-type and mutant β-catenin

FCS is a powerful quantitative microscopy method for measuring local concentrations and diffusional mobilities of fluorescent molecules in cells and tissues, e.g., to determine Wnt ligand-receptor interactions in the cell membrane (Eckert et al., 2020). To simultaneously monitor the dynamics of wild-type Clover-tagged and mutant Cherry-tagged β-catenin of HCT116 cells clone #37, we used FCS with detection in two color channels. With this method, we record the

fluorescence intensity emanating from a tiny observation volume (ca. 1 fL) as a function of time. For each cell studied, two measurements were performed, with the observation volume first positioned into the cytosol and then into the nucleus. Thus, we focused on the freely diffusing β-catenin fraction, which mediates Wnt signaling, and excluded the membrane-bound fraction, which is responsible for cell-cell adhesion and has been previously shown by FRAP to tightly interact with cadherins, which markedly reduces its mobility.

From the intensity time traces in the two color channels, autocorrelation functions were calculated and fitted with model functions (Figure S6) to extract two parameters, the diffusional correlation time and the correlation amplitude (Zemanová et al., 2003). The correlation time is inversely proportional to the diffusion coefficient, D, of the fluorescent molecules. For this conversion, we performed calibration FCS experiments using fluorescent dye molecules with known D values as reference samples (see Methods). According to the Stokes-Einstein law, the diffusion coefficient is inversely related to the linear extension of the diffusing entity and thus to the cube root of its volume/molecular mass. Thus, measurement of D values provides size information. The correlation amplitude is inversely proportional to the average number of molecules, N, in the observation volume. The calibration experiment with dye molecules mentioned above also allows us to determine the effective volume, V_{eff}, from which the fluorescence emanates, so that the molecule concentration, c, in the observation volume can simply be calculated as $c = N / V_{eff}$. In addition to autocorrelation analysis, we calculated cross-correlation functions to identify correlated intensity fluctuations in the two color channels. These will appear if the Clover and Cherry labeled β-catenin molecules co-diffuse, i.e., bind to each other and migrate in concert through the observation volume. Cross-correlation amplitudes between wild-type Clover-tagged and mutant Cherry-tagged β-catenin were always found to be zero within the experimental error, implying that these two β-catenin variants diffuse independently and do not associate to any significant degree (Figure S6).

On the basis of FCS experiments in the cytosol of more than 40 cells, we calculated a median D value of 10.6 ± 1.8 $\mu m^2\ s^{-1}$ for mutant Cherry-tagged β-catenin, which is significantly smaller than the one of wild-type Clover-tagged β-catenin (D = 17.3 ± 6.1 $\mu m^2\ s^{-1}$, Figure 6A). The ratio of diffusion coefficients indicates that mutant Cherry-tagged β-catenin diffuses as part of a larger complex, with a more than four-fold larger volume/overall mass than wild-type Clover-tagged β-catenin. For Clover and Cherry overexpressed in HCT116 cells, we measured D = 43 ± 8 $\mu m^2\ s^{-1}$ in the cytosol (data not shown). Taking this number and dividing it by the cube root of the molecular mass ratio between wild-type Clover-tagged β-catenin and Clover (120 kDa : 26 kDa), we obtain an estimated D = 26 ± 5 $\mu m^2\ s^{-1}$ for the tagged β-catenin, which is on the high

end of the distribution of *D* values of the respective ensemble (Figure 6A). Thus, Clover-tagged β-catenin may diffuse as an individual entity or as part of a smaller complex (compared to the one that mutant Cherry-tagged β-catenin is bound to).

From the autocorrelation amplitudes in the green and red color channels, the concentrations of wild-type Clover-tagged β-catenin and mutant Cherry-tagged β-catenin were determined as 32 ± 9 nM and 75 ± 11 nM (medians of distributions over more than 40 cells, Figure 6A and B). These data agree well with previous measurements in the RKO cell line, which revealed β-catenin concentrations of ~52 nM upon Wnt3A stimulation (Hernández et al., 2012).

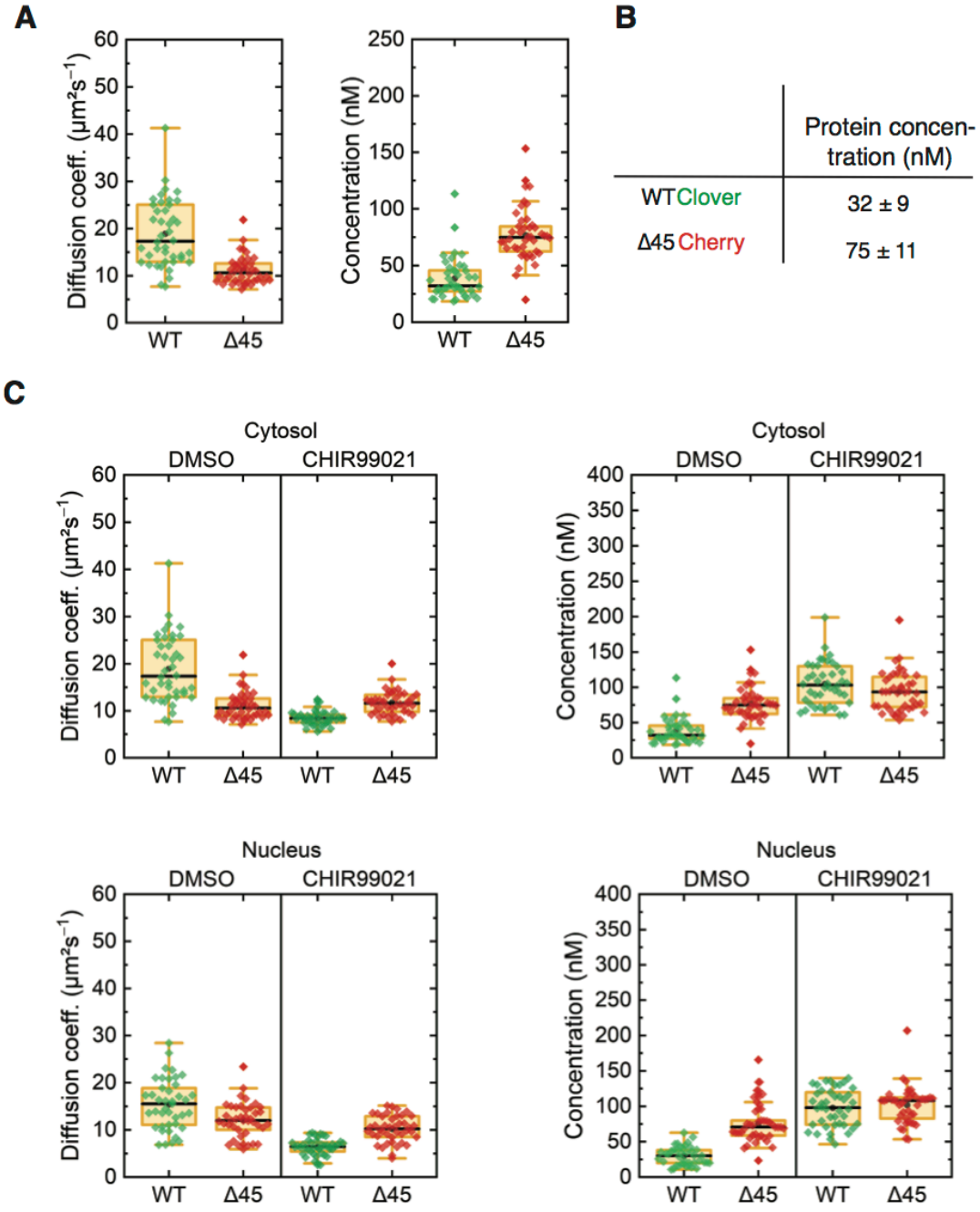

Figure 6: FCS autocorrelation analyses reveal differences in the dynamics and concentrations of wild-type and mutant β-catenin. (A) Diffusion coefficients (left) and concentrations (right) of Clover-tagged wild-type β-catenin and Cherry-tagged mutant β-catenin in the cytosol of HCT116 β-catenin$^{wtClover/\Delta45Cherry}$. (B) Protein concentrations (medians of the distributions shown in panel a). C) Correlation times and amplitudes of Clover-tagged wild-type β-catenin and Cherry-tagged mutant β-catenin measured on HCT116 β-catenin$^{wtClover/\Delta45Cherry}$ cells that were treated for 14 – 26 hours with either 10 µM CHIR9901 or DMSO as control. The FCS observation volume was positioned (top) in the cytoplasm and (bottom) in the nucleus. Each data point represents a 120-s FCS measurement in a single cell. In total, more than 40 cells per condition were measured in three independent experiments per box plot.

Next, we were interested whether activation of the Wnt signaling pathway had an impact on the diffusional dynamics of wild-type and mutant β-catenin. Therefore, FCS measurements were performed in the presence of the GSK3β inhibitor CHIR99021, which induces canonical Wnt signaling as depicted in Figure 4A. Under control conditions (DMSO), wild-type β-catenin was again less abundant and diffused faster than mutant β-catenin in the cytosol (Figure 6C). Interestingly, treatment with CHIR99021 changed the diffusion coefficients and concentrations of wild-type β-catenin so that they became similar to the ones of mutant β-catenin. By contrast, the diffusional dynamics and concentration of the mutant isoform were unaffected by GSK3β inhibitor treatment. Essentially the same effects were obtained for both isoforms in the nuclear fraction (Figure 6C). These observations suggest that, by applying the drug, wild-type β-catenin was also incorporated into a larger complex. The increased concentration suggests that complex formation reduces the probability of β-catenin degradation. Together, these results indicate that GSK3β inhibition renders the concentration and diffusional dynamics of wild-type β-catenin such that they are similar to those of the mutant isoform.

APC truncation affects only the dynamics of the wild-type β-catenin isoform

APC mutations are frequently found in colorectal cancer and define the onset of the transition from adenoma to carcinoma. The complete loss of *APC* is very rare, truncating mutations lacking the C-terminal domain are, however, frequently observed(Cancer Genome Atlas Network, 2012; Fearnhead et al., 2001). Hence, we engineered cell lines carrying mutant truncated APC using CRISPR/Cas9 editing in the biallelic tagged HCT116 clone #37, and quantitatively assessed the impact of APC truncations on wild-type and mutant β-catenin protein in the same cell.

A sgRNA (sgAPCb) was designed by E-CRISP to target the mutation cluster region (MCR) in exon 15 of *APC* (Zhan et al., 2019; Heigwer et al., 2014), introducing a premature stop codon (Figure 7A). Edited single clones were verified by amplicon sequencing confirming the homozygous *APC* mutation (Figure 7A). Subsequently, FCS measurements were performed to study the cytosolic and nuclear fractions of both parental HCT116 $\beta\text{-catenin}^{wtClover/\Delta45Cherry}$ and HCT116 $\beta\text{-catenin}^{wtClover/\Delta45Cherry}$ APC^{LOF} (sgAPC) cells. In the cytosol (Figure 7B) and also in the nucleus (Figure S7) of APC^{LOF} cells, both the concentration and diffusional dynamics of wild-type β-catenin were similar to those found for mutant β-catenin in both control and APC^{LOF} cells. Furthermore, treatment with the GSK3β inhibitor had no additional effect, neither on the dynamics nor on the concentration, independently of the condition. Thus, truncation of APC or GSK3β inhibition affect the dynamics and abundance of wild-type β-catenin. Interfering with Wnt signaling at the level of the destruction complex results in wild-type β-catenin phenocopying the mutant β-

catenin isoform, suggesting that the behavior of mutant β-catenin is not intrinsic to the isoform, but can be modulated by changing the signaling state of the cell.

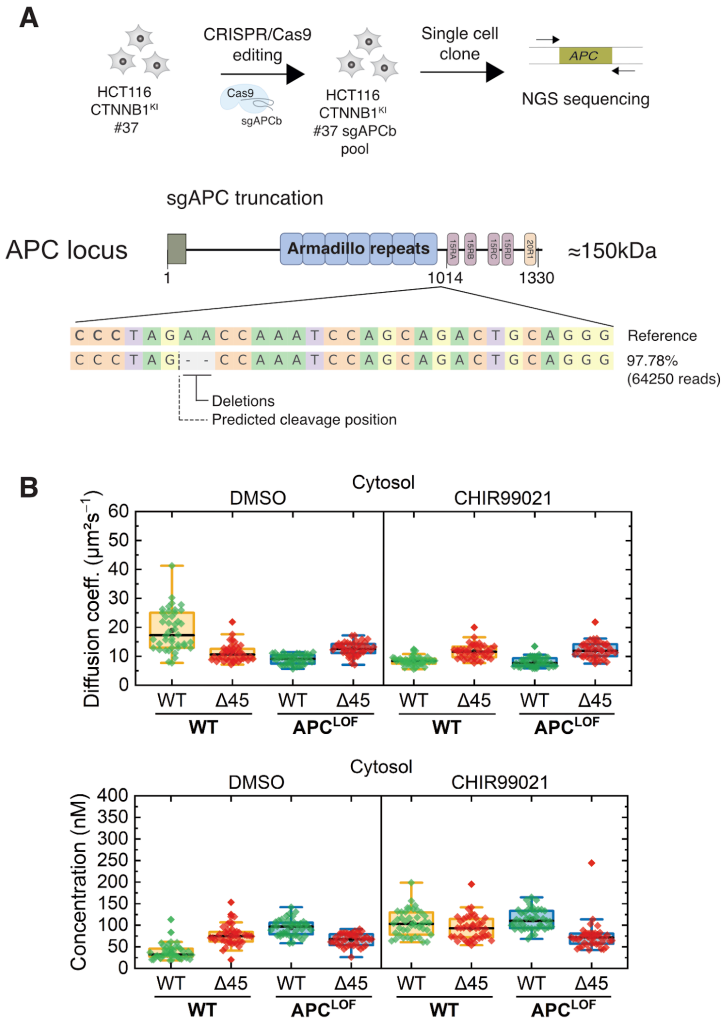

Figure 7: Truncation of APC affects abundance and diffusional dynamics of wild-type but not mutant β-catenin in the cytosol. (A) Schematic representation of the *APC* locus and target site of sgACP in the mutation cluster region (MCR) domain. (B) HCT116 β-catenin$^{wtClover/\Delta45Cherry}$ and sgAPC targeted clone (APC^{LOF}) cells were treated for ~16 hours with either 10 μM CHIR9901 or DMSO as control. Subsequently, FCS measurements were performed in the cytosol (data shown here) and in the nucleus (data shown in Figure S7). Each data point in the box plots represents a result from a 120-s FCS measurement in a single cell. Per box plot, more than 40 cells were investigated in three independent experiments.

DISCUSSION

How disease-causing genetic alleles affect protein function has remained a subject of intense research (Sahni et al., 2015). Mutations in β-catenin that activate the Wnt pathway occur in about 5% of colorectal and more than 25% of liver and uterine tumors (Hoadley et al., 2018; Sanchez-Vega et al., 2018) Nevertheless, the investigation of its biochemical properties has been hampered by the lack of suitable tools to study its function at a physiological level. Here we generated cellular models to simultaneously analyze wild-type and oncogenic mutant alleles of β-catenin. We took advantage of the recent developments in CRISPR/Cas9 technology to engineer allele-specific endogenously β-catenin fused to a fluorescent protein. Thereby, we successfully generated an endogenously tagged β-catenin cell line carrying mClover-tagged wild-type and mCherry-tagged mutant β-catenin at the same time. While tagging of proteins can interfere with protein functions, it can also lead to accumulation of the protein and overactivation of the respective pathway. In line with our results, previous overexpression studies showed that C-terminal tagging of β-catenin did not affect any of its functions (Giannini et al., 2000; Jamieson et al., 2011; Kafri et al., 2016; Krieghoff et al., 2006). Accordingly, all generated clonal cell lines with one or both tagged alleles had the same proliferation capacity (Figure 2A). By contrast, inactivation of β-catenin or canonical Wnt signaling in HCT116 cells has been previously shown to inhibit proliferation (Scholer-Dahirel et al., 2011; Voloshanenko et al., 2013). In addition, fluorescently tagged β-catenin did not affect Wnt pathway regulation (Figure 2E). It has been previously demonstrated, the region responsible for adhesion lies in the central part of β-catenin and not in the C-terminus (Valenta et al., 2012; Xing et al., 2008). Therefore, the likelihood of C-terminal tagging affecting this function is rather small. Indeed, we found that β-catenin adhesive function was not affected (Figure 2C, 2D). Due to the limited availability of technologies, previous studies used overexpression of fluorescently tagged β-catenin to analyze its kinetics (Jamieson et al., 2011; Kafri et al., 2016; Krieghoff et al., 2006). Single cell analysis of low level expressed β-catenin in real time revealed a cell-to-cell variability regarding the amount of β-catenin and the time when β-catenin accumulated (Kafri et al., 2016).

The advancement in genome editing technologies such as CRISPR/Cas9 emerged as a valuable tool for endogenous tagging of proteins (Cong et al., 2013; Dambournet et al., 2014; Mali et al., 2013). Several reports described diverse approaches to increase the editing efficiency and to identify the crucial points for successful donor integration (Lackner et al., 2015; Martin et al., 2019; Yang et al., 2014). Based on these guidelines we chose the design of our two donor templates 180bp homology arms for the insert of around 3 kbp. Surprisingly, the integration of the two donor templates was different, with Clover having an about 12-fold better integration efficiency

than Cherry (Figure S1B). This might indicate that the efficiency of HDR depends not only on homology arms but also on the integrated sequence, however, we cannot exclude that these differences might be due to different antibiotic cassettes.

β-catenin plays an important role not only in Wnt signaling but also in cell adhesion, in which it links the adhesion complex to the actin cytoskeleton via its interaction with the actin-binding protein α-catenin (Rimm et al., 1995). Since the different functions require distinct localization, β-catenin can be found in at least two distinct pools, one at the cell membrane and one that can shuttle between the cytosol and nucleus. Whether both pools originate from a common pool or from two independent pools, and how these reservoirs regulate each other is still a matter of debate. Accordingly, Valenta et al. showed *in vivo* that it is possible to affect one function of β-catenin without interfering with the other (Valenta et al., 2012, 2011). Moreover, different molecular forms of β-catenin have been described, which demonstrated that most cytosolic β-catenin exists in a monomeric form, whereas dimers of α-catenin and β-catenin interacted mainly with cadherin (Gottardi and Gumbiner, 2004). Interestingly, our immunoprecipitation and FCS analyses indicate that wild-type and mutant β-catenin are found in two separate pools. We observed that β-catenin is mobile in both compartments, whereas mutant β-catenin is found in higher molecular weight complexes and has a lower affinity for E-cadherin. Consistently, if the mutant form is less abundant at the cell membrane, this might explain an increased concentration of β-catenin in the cytosol and nucleus as observed by FCS (Figure 6C).

FCS measurements revealed that wild-type β-catenin diffuses faster than the mutant isoform in the cytoplasmic and the nuclear compartments. This difference was abolished when we applied the GSKβ-inhibitor or introduced an APC deletion, resulting in slower diffusion and lower abundance of wild-type β-catenin, similar to the mutant isoform. The changed diffusional dynamics upon activation of canonical Wnt signaling is likely due to the onset of interactions with members of the destruction complex or with transcription factors, respectively. Along this line, FRAP analysis demonstrated that TCF4, APC, Axin and Axin2 reduced β-catenin mobility and nucleo-cytoplasmic shuttling suggesting that these interaction partners control the subcellular localization of β-catenin by sequestering it in the respective compartment (Krieghoff et al., 2006). Accordingly, Goentoro and Kirschner demonstrated that fold changes of β-catenin rather than molecule numbers regulate Wnt signaling (Goentoro and Kirschner, 2009). A recent manuscript demonstrated that wild-type β-catenin resides in slow-diffusing complexes in the cytosol and nucleus in HAP1 cells (de Man et al., 2020), suggesting that Wnt activation regulates β-catenin dynamics by a combination of destruction complex modifications, and modulating nucleoplasmic shuttling and nuclear retention.

In summary, we engineered, to our knowledge, the first biallelic tagged cell model carrying a different fluorescent fusion protein on each allele, demonstrating the feasibility of our one-step tagging strategy to analyse the consequences of genetic variants. β-catenin knock-in cell lines provide a powerful tool for investigating β-catenin's role in the canonical Wnt signaling, and also in adhesion. Due to these properties of β-catenin, the cell models can serve to evaluate both functions in parallel on the endogenous level. Cell models of wild-type and mutant variants can also be used for drug discovery, identifying small molecules that only interfere with mutant, but not wild-type β-catenin, thereby circumventing side effects that are often associated with interfering with homeostatic levels of Wnt signaling. In general, bi-allelic tagging of genetic variants in their endogenous locus can open new avenues towards understanding and possibly targeting disease-causing variants in a broad spectrum of cellular and organismal phenotypes.

METHODS

Cell Culture

The parental colon cancer HCT116 (β-catenin$^{wt/\Delta 45}$) cell line was purchased from the American Type Culture Collection. HCT116 β-catenin$^{wt+/-}$ cells were obtained from Horizon Discovery. Cells were culture in McCoy's medium (GIBCO) supplemented with 10% fetal bovine serum (Biochrom GmbH). Cells were grown at 37°C and 10% CO_2 in a humidified atmosphere. Cells were tested for cross-contamination using SNP profiling by a Multiplex human Cell Authentication (MCA) assay (Multiplexion) and regularly checked for Mycoplasma contamination.

Transfection

Transient transfections were performed using TransIT-LT1 Transfection Reagent (731-0029; VWR) for DNA plasmids and Lipofectamine RNAiMax (Thermo Fisher Scientific) for siRNAs according to the manufacturer's protocol. 15-25nM Dharmacon siRNAs (Horizon discovery) and 5-10nM Ambion siRNAs (Thermo Fisher) were used for reverse siRNA transfection (Table S1).

Small molecule inhibitors

GSK-3β inhibitor CHIR99021 (Cat. No. 361571) and Tankyrase inhibitor XAV939 (Cat. No. 575545) were obtained from Merck-Millipore. ICG001 (Cat. No. Cay16257-1) was obtained from Biomol. DMSO was used as the vehicle control.

Western blot and co-immunoprecipitations assays

Whole cell lysates were extracted using a buffer containing non-ionic detergents such as Triton X-100 or NP-40, supplemented with protease inhibitors (Roche). Protein concentration was determined using BCA protein assay kit (Thermo Fisher Scientific) according to the manufacturer's instructions. Samples were loaded on 4-12% NuPAGE Bis-Tris gels or 3-8% NuPAGE Tris acetate gels (Thermo Fisher Scientific) and transferred to the nitrocellulose membranes (GE Healthcare, GE10600002) following standard western blotting procedure. Antibodies and their dilutions are listed in Table S2. For immunoprecipitation extracts were pre-cleared by incubation with binding control magnetic agarose beads (Chromotek) for 30 minutes at 4˚C. Clover- and Cherry-tagged proteins were immunoprecipitated by incubation with either GFP- or RFP-Trap magnetic beads (Chromotek) for 1 h at 4˚C with rotation. For E-cadherin and β-catenin IPs extracts were incubated with control or respective antibody (Table S2) together with Dynabeads Protein G magnetic beads (Thermo Fisher Scientific) for 12 h at 4˚C.

sgRNA design and cloning

sgRNAs sequences targeting the *CTNNB1* and *APC* genes were designed using the E-CRISP (Heigwer et al., 2014), synthesized by Eurofins and cloned into the px459 plasmid (#62988, Addgene) (Table S3), according to a previously described protocol (Mali et al., 2013). To generate donor plasmids the desired homology arm's regions and epitope tag (either V5 or FLAG) were synthetized by Invitrogen GeneArt Gene Synthesis and cloned into the vector backbone pMK-RQ. The Clover PGK-HygR and Cherry PGK-BRS were cloned from the published vectors pMK278 (Addgene #72794) and pMK282 (Addgene # 72798), respectively (Natsume et al., 2016). Oligonucleotides and PCR primers are listed in Table S5.

Generation and validation of allele-specific endogenously tagged β-catenin cell lines

HCT116 cells were transfected with px459sgCTNNB1 and the two donor template encoding plasmids KOZAK_FLAG_mClover3 and KOZAK_V5_mCherry using TransIT (731-0029; VWR) according to manufacturer's instructions. As controls, each donor template was also transfected alone together with px459sgCTNNB1 to generate single-tagged β-catenin cells and to adjust gates for FACS sorting. After 72h, cells were selected with 2 µg/ml puromycin (P9620, Sigma). 48h later, 100µg/ml hygromycin 10687010, Gibco/Thermo Fisher Scientific) and 10µg/ml blasticidin (R21001, Life Technologies GmbH) were added to select edited cells for five days. Subsequently, surviving cells were sorted as single cell clones by FACS into 96 well plates for cultivating. To validate correctly endogenously tagged β-catenin clones genotyping was performed. Genomic DNA was extracted with phenol-chloroform. Different primer pair combinations were designed for genotyping (Table S5). Primer pair (a) binds to the endogenous β-catenin locus flanking the donor cassette indicating homo- or heterozygous integration of the donor template. Primer pairs (b), (b') and (c) bind outside and inside the donor indicating the correct in-frame integration. Primer pair (d) binds inside the donor indicating which fluorophore was integrated. PCR products were analyzed by agarose gel-electrophoresis.

TCF4/Wnt-reporter activity assay

To determine Wnt signaling activity, the luciferase-based dual Wnt reporter assay was performed as described previously (Demir et al., 2013). Briefly, cells were transfected with plasmids encoding the TCF4-driven firefly luciferase and actin-promoter driven Renilla luciferase as control (Table S3). Dual-luciferase readout was performed 48 hrs after transfection using Mithras LB940 plate reader (Berthold Technologies). Wnt activity was calculated by normalization of the TCF4/Wnt-luciferase values to the actin-Renilla values.

RT-qPCR

Total RNA from cell pellets was isolated with the RNeasy Mini kit (Qiagen) according to the manufacturer's protocol. RNA was reverse-transcribed into cDNA using the RevertAid H Minus First Strand cDNA Synthesis kit (Thermo Fisher Scientific). qPCR was performed using the Universal probe library (Roche) with the LightCycler 480 (Roche) instrument according to the manufacturer's instructions). A list of primers used in this paper for qPCR is shown in Table S4.

Immunofluorescence assays

Sterile coverslips (Thermo Fisher Scientific) were placed into 12 well plates and cell suspension was added. One day later, cells were treated with the indicated drugs for 20 - 24 h. Cells were fixed using 4% PFA (VWR) for 20 minutes at room temperature. For antibody staining, cells were permeabilized with 0.25% Triton/PBS. After several washing steps, cells were blocked for 1 h with 5% goat serum (v/v) and 5% BSA (v/v) in PBS at room temperature. After overnight incubation with the primary antibody at 4℃, cells were incubated with fluorescently labeled secondary antibodies (1:250) for 1 h at room temperature in the dark. Antibodies were diluted in PBS with 5% goat serum (v/v) and 5% BSA (v/v). Finally, cover slips were gently transferred onto microscope slides (Carl Roth GmbH) and fixed with Vectashield mounting media containing DAPI solution (Biozol Diagnostica). Fluorescence images were acquired with a Leica TCS SP5 confocal microscope. For live cell imaging, cells were added into µ-slide with a glass bottom (Ibidi) and staining was performed as described. For automated microscopy cells were seeded into 384 well plates and subjected to fixation using the CybiWell Vario robotic system. Fluorescence images were acquired using InCell Analyzer 2200 microscope (GE Healthcare) at 20X magnification in three channels (DAPI, Cy3 and FITC) with four sites per well.

Image analysis

Image analysis of automatic microscopy was performed using R package EBImage (Pau et al., 2010) and adapted based on previous analysis methods (Carpenter et al., 2006; Fuchs et al., 2010). Nuclei and cell body were segmented and features for intensity, shape and texture were extracted for each cell based on the DAPI, actin and tubulin staining. Features were then summarized per experiment by mean calculation over all cells. As a proxy for cell count, the number of segmented nuclei was used. Images were assembled using Affinity Designer, Biorender and Adobe Illustrator.

Fluorescence correlation spectroscopy

For FCS measurements, HCT116 cells were cultured without phenol red and seeded in fibronectin (Sigma-Aldrich, St. Louis, MO) coated 8-well Nunc Lab-Tek chambered cover glass (Thermo Fisher Scientific). To this end, fibronectin was diluted at 50 µg/ml in Dulbecco's phosphate buffered saline (DPBS, no calcium, no magnesium, Sigma Aldrich). Each well of the 8-well chamber was incubated with 200 µL of the solution for at least 1 h at room temperature. Afterwards, the solution was removed by aspiration, and the wells were allowed to dry. Fibronectin coated chambers were either used directly afterwards or stored at 4°C for a maximum of 1 – 2 weeks and washed with DPBS directly before use. Upon treatment with drugs, the cell culture medium was replaced with a drug-containing medium for ~16 – 26 hours before the measurements. FCS measurements were started ~12 h after seeding the cells at 37°C and with 5% CO_2.

For FCS analysis, intensity time traces of 120 s duration were acquired in two color channels for 120 s each by using a home-built confocal microscope described previously (Eckert et al., 2020). Clover and Cherry were excited with pulsed 470- and 561-nm laser light of typically 3 µW (1.5 kW/cm^2) and 5 µW (2.8 kW/cm^2), respectively. The emission was filtered by 525/50 nm and 607/37 nm (center/width) band pass filters (BrightLine, Semrock, Rochester, NY). For data acquisition, the observation volume of the microscope was first positioned into the cytoplasm and directly afterwards into the nucleus. The intensity decrease during the measurement due to photobleaching was compensated as described previously (Dörlich et al., 2015). Then, autocorrelation and cross-correlation functions were calculated from the time traces, and correlation amplitudes and times were extracted by fitting a model function to the correlation functions that describes free diffusion of fluorescent particles through an observation volume shaped as a three-dimensional Gaussian function(Gao et al., 2017). Two correction factors were applied to the correlation amplitudes of each individual cell measurement to account for photobleaching and uncorrelated background due to cellular autofluorescence. The correction for photobleaching was described recently(Eckert et al., 2020). To correct for autofluorescence according to (Foo et al., 2012), we measured background intensities in the cytosol and in the nucleus for ensembles of more than 15 cells of lines #45 and #33, both under control conditions (DMSO) and with drug treatment (CHIR99021). For each cellular experiment, the correction factor was calculated using the median intensity of the respective ensemble. Finally, the (microscope-dependent) correlation times and corrected amplitudes were converted into (microscope-independent) diffusion coefficients and concentrations, which are reported in this work. To enable this conversion, we carried out careful calibration experiments using solutions of organic dyes (Alexa 488 and Alexa 546, Thermo Fisher Scientific) with well-known diffusion coefficients and

concentrations. Furthermore, FCS measurements on fluorescent proteins (eGFP, Clover, Cherry) overexpressed in HCT116 WT cells were performed to obtain estimates of the molecular mass of the diffusing entities.

ACKNOWLEDGEMENTS

We are grateful to K.E. Boonekamp and S. Redhai for providing critical comments on the manuscripts. We would like to acknowledge all members of the Boutros group and of the SFB1324 for helpful discussions. We thank F. Zhang, M. Waterman and D. Virshup for plasmids, which were obtained via Addgene. We are grateful to support by the Excellence Cluster CellNetworks Core Facilities. This work was funded by the Deutsche Forschungsgemeinschaft (DFG, German Research Foundation) Project No. 331351713 – SFB 1324 “Mechanisms and Functions of Wnt signaling” (Projects Z03 to M.B. and A06/Z02 to G.U.N).

AUTHOR CONTRIBUTIONS

M.B. and G.A. designed the study; G.A. designed and generated β-catenin alleles in cell lines, characterized and studied different alleles in canonical Wnt signalling; O.V., D.K. characterization endogenous β-catenin alleles; A.E. performed the FCS experiments and analysis; M.B., G.U.N., D.K., O.V., G.A., A.E., wrote the manuscript. M.B. and G.U.N. supervised the study.

COMPETING INTERESTS

The authors declare no competing financial interests.

SUPPLEMENTARY TABLES

Table S1. siRNAs

Target gene	Supplier	Catalogue #	Sequence
UBC	GE Healthcare Dharmacon/Horizon	MU-019408-01-0002	#1 GTGAAGACCCTGACTGGTA #2 AAGCAAAGATCCAGGACAA #3 GAAGATGGACGCACCCTGT #4 GTAAGACCATCACTCTCGA
Non targeting	GE Healthcare Dharmacon/Horizon	D-001810-02	UGGUUUACAUGUUGUGUGA
Control	Ambion	S29712	
GFP	GE Healthcare Dharmacon//Horizon	D-001300-01-05	GCAAGCTGACCCTGAAGTTC
CTNNB1	Ambion	S438	CUGUUGGAUUGAUUCGAAAtt
Cherry	IDT	Custom design	#3 rCrArU rGrGrC rCrArU rCrArU rCrArA rGrGrA rGrUrU rCrArU rG

Table S2. Antibodies

Antibody	Company	Catalogue #	Species	Dilution
β-actin HRP	Santa Cruz Biotechnology	47778	rabbit	1:250000
β-actin	Santa Cruz Biotechnology	47778	rabbit	1:40000
β-catenin	BD Biosciences	610154	mouse	1:2000
Cherry	Clontech	632543	mouse	1:1000
GFP	Invitrogen	332600	mouse	1:1000
E-Cadherin	BD Biosciences	610182	mouse	1:1000
V5	Rockland	600-401-378	rabbit	1:4000
Normal IgG	Cell Signaling Technology	2729	rabbit	
IgG1 K isotype control	eBioscience	16-4714-81	mouse	
Anti-mouse IgG-HRP	Jackson ImmunoResearch	115-035-003	Goat	1:10000
Anti-rabbit IgG-HRP	Jackson ImmunoResearch	111-035-003	Goat	1:10000

Table S3. Plasmids

Plasmid	Reference	Comments
Actin-Renilla luciferase	(Nickles et al., 2012)	TCF4/Wnt reporter assay
TCF4/Wnt-reporter	(Demir et al., 2013)	TCF4/Wnt reporter assay
px459sgCTNNB1	This study	sgRNA: TGACCTGTAAATCATCCTTT
KOZAK_FLAG_mClover3	This study	Overexpression plasmid
KOZAK_V5_mCherry	This study	Overexpression plasmid
px459sgAPC#b	This study	sgRNA: TAGAACCAAATCCAGCAGA
pSpCas9(BB)-2A-GFP (PX458)	Addgene #48138	Control vector
pMK-RQ HA-FLAG-mClover-PGK-HygRHA	This study	Donor template
pMK-RQ HA-V5-mCherry-PGK-BRS-HA	This study	Donor template

Table S4. Primers and Roche UPL index used in qPCR experiments

Gene	UPL Probe #	Forward (5'-3')	Reverse (5'-3')
Clover	148	TATATCACGGCCGACAAGC	GTTGTGGCGGATCTTGAAGT
Clover	41	AACTTCAAGATCCGCCACAACG	CGTGCTGCTTCATGTGGT
Cherry	161	CTACGAGGGCACCCAGAC	CGTACATGAACTGAGGGGACA
Cherry	152	GTGACCGTGACCCAGGAC	GTGACCGTGACCCAGGAC
AXIN2	88	AGAGCAGCTCAGCAAAAAGG	CCTTCATACATCGGGAGCAC
GAPDH	60	AGCCACATCGCTCAGACAC	GCCCAATACGACCAAATCC
UBC	11	ACCAGCAGAGGCTGATCTTT	TCTGGATGTTGTAGTCTGACAGG
CTNNB1	21	AGCTGACCAGCTCTCTCTTCA	CCAATATCAAGTCCAAGATCAGC

Table S5. Oligonucleotides

Name	Primer Sequence (5'-3')
3XFLAG_F	AGCTGGCCTGGTTTGATACTGACCTGGACTATAAGGACCACGACG GAGACTA
3XFLAG_R	CGATCCGCCACCGCCAGAGCCACCTCCGCCTGAACCGCCACCAC CTGACTTATCGTCATCGTCTTTGTAATCAATATC
GFP_R	CCCAAACTGGCTTTTTAAAACTTCTTTACTTGTACAGCTCGTCCATG CCGAGAGTGA
GFP_F	TCAGGTGGTGGCGGTTCAGGCGGAGGTGGCTCTGGCGGTGGCG GATCGCCGGTCGCCACCATGGTGAGCAAGG
RHA2_F	CGGCGGCATGGACGAGCTGTACAAGAGAAGTTTTAAAAAGCCAGT TTGGG
RHA2_R	CTATGACCATGATTACGCCAAGCTTTTCTTGAGTCACTCCCAAAAT CCA
CHERRY 2_R	CCCAAACTGGCTTTTTAAAACTTCTCTTGTACAGCTCGTCCATGCC G
CHERRY2_F	TCAGGTGGTGGCGGTTCAGGCGGAGGTGGCTCTGGCGGTGGCG GATCGATGGTGAGCAAGGGCGAGGA
V5_2_R	CGATCCGCCACCGCCAGAGCCACCTCCGCCTGAACCGCCACCAC CTGACGTAGAATCGAGACCGA
V5_2_F	GCTGGCCTGGTTTGATACTGACCTGGGTAAGCCTATCCCTAACC
LHA2_R	GGGATAGGCTTACCCAGGTCAGTATCAAACCAGGCCAG
LHA2_F	GTTGTAAAACGACGGCCAGTGAATTAAGCTTGACAGGGGTAAATG CAGAGTGTTCAG
PGK_REV	CCTCCCCTACCCGGTAGAATTT
BCAT_GDNA_R	AACAAGCAAGGCTAGGGTTT

BCAT_CHERRY_R	AGCCGTACATGAACTGAGG
BCAT_CHERRY_F	AGCCGTACATGAACTGAGG
BCAT_GDNAF	TCACTGCCTAGGTGGTCACA
BCAT_GFPF	ACCACTACCAGCAGAACAC
BCAT_GFPR	TCGTGCTGCTTCATGTGGT
SGBCAT_FSEQ	TGGCACCACTTCCCGC
SGBCAT_RSEQ	CTGTGGGCGAGGCCAT
BCAT_TAG2_FW	AAATAGTGCCTTTCCTTAGTAC
BCAT_TAG2_R	AATTAGTGTTCTACACCATTAC
ATG_BCAT1F	AGAAAAGCGGCTGTTAGTCACTG
ATG_BCAT2_F	TGTTAGTCACTGGCAGCAACAGTC
BCAT_TAG3_F	AGCAACAGTCTTACCTGGACTCTG
BCAT_ATG3_R	GCATCTGTGATGGTTCAGCCAAA
BCAT-TAG3_F	ATGAAACCACTAAAGCGCAGATTC
BCAT_TAG3_R	TCTTGAAGCATCGTATCACAGCAG
CLOVER_R	CGTTGTGGCGGATCTTGAAGTT

CLOVER_F	AACTTCAAGATCCGCCACAACG
CHERRY_MID_R	CCATGGTACGACACTGCATT
CHERRY_MID_F	AATGCAGTGTCGTACCATGG

SUPPLEMENTAL FIGURES

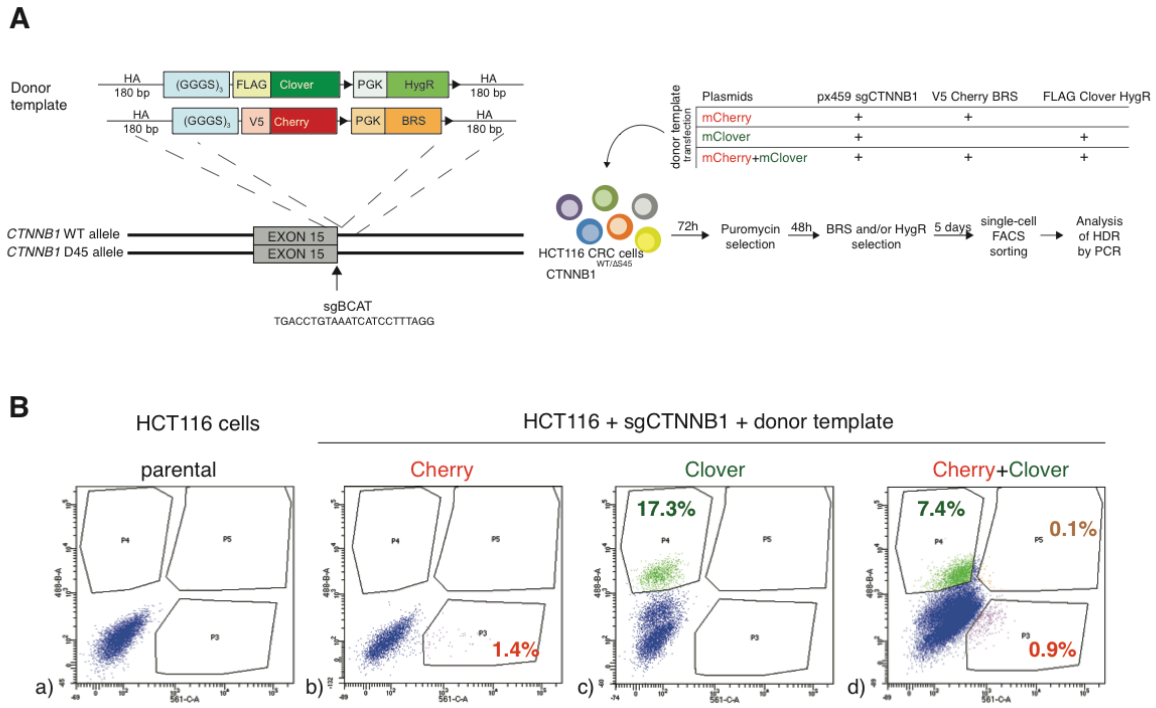

Figure S1: Generation of endogenous fluorescently tagged β-catenin cell lines. (A) Schematic representation of *CTNNB1*/β-catenin tagging strategy and workflow of bi-allelic β-catenin tagged HCT116 cells generation (B) The editing efficiency between the two donor templates was different. The donor template Clover was more efficiently integrated than the Cherry one. (a) Parental HCT116 cells were used as "unstained" sample for FACS analysis (b) HCT116 cells transfected with sgCTNNB1 and Cherry donor template were used to define the gate P3 (mCherry+ cells), (c) HCT116 transfected with sgCTNNB1 and Clover donor template were used to set the gate P4 (mClover+ cells), (d) edited cells transfected with sgCTNNB1 and both Cherry and Clover donor templates are double-positive (gate P5). Percentages of positive cells are shown in each panel.

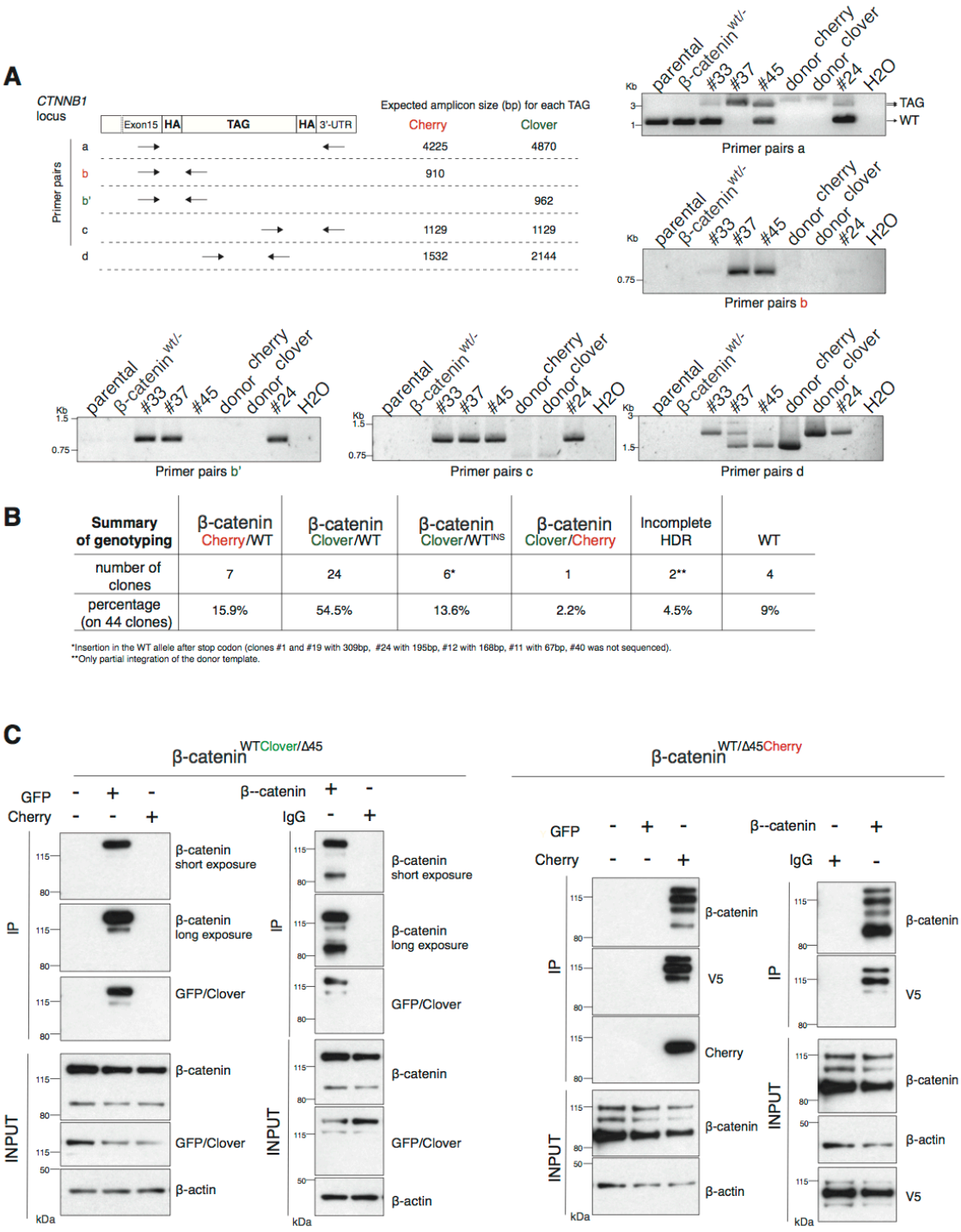

Summary of genotyping	β-catenin Cherry/WT	β-catenin Clover/WT	β-catenin Clover/WT^{INS}	β-catenin Clover/Cherry	Incomplete HDR	WT
number of clones	7	24	6*	1	2**	4
percentage (on 44 clones)	15.9%	54.5%	13.6%	2.2%	4.5%	9%

*Insertion in the WT allele after stop codon (clones #1 and #19 with 309bp, #24 with 195bp, #12 with 168bp, #11 with 67bp, #40 was not sequenced).
**Only partial integration of the donor template.

Figure S2: Generation and validation of endogenously fluorescent-tagged β-catenin in HCT116 colon cancer cells. (A) The table indicates primers used for genotyping of single cell clones. PCR analysis shows genotyping of HCT116 single cell clones #33, #37, #45 and #24. Parental HCT116 β-catenin$^{wt/\Delta 45}$, HCT116 β-catenin$^{wt/-}$ and donor templates were used as controls. (B) Table summarizing the obtained HCT116 single clones with their according genotypes. (C) Immunoprecipitation using HCT116 β-catenin$^{wtClover/\Delta 45}$ (clone #33 - left) and β-catenin$^{wt/\Delta 45Cherry}$ (clone #45 - right) were performed with GFP, Cherry and control beads or with β-catenin antibody, followed by western blotting with the indicated antibodies. β-actin was used as a oading control. Representative results from three independent experiments are shown.

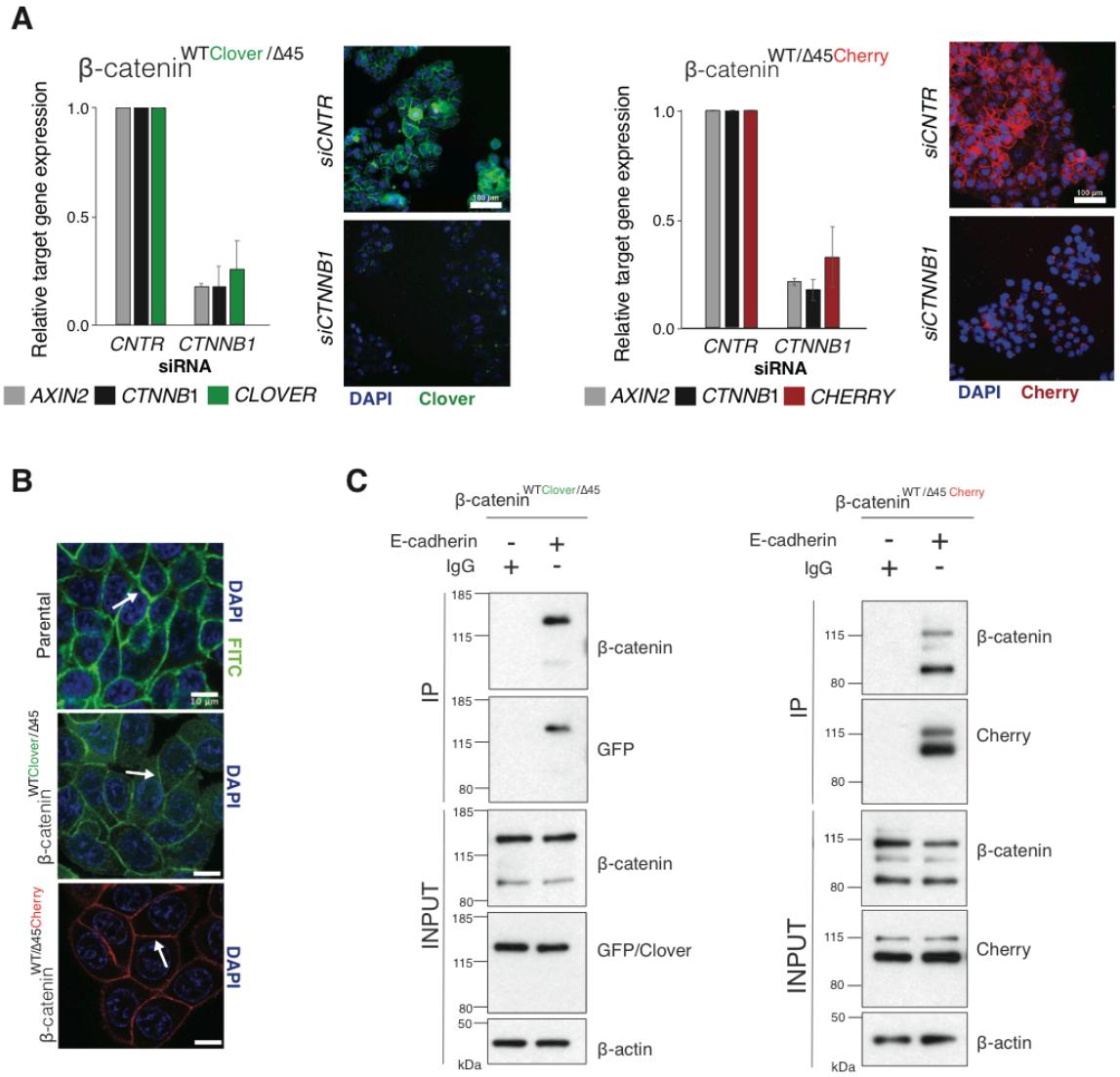

Figure S3: Validation of the physiological function of fluorescently tagged β-catenin. (A) In HCT116 β-catenin$^{wtClover/\Delta45}$ and β-catenin$^{wt/\Delta45Cherry}$ mRNA-levels of *CTNNB1, AXIN2*, *CHERRY* and *CLOVER* were determined by RT-qPCR upon silencing of *CTNNB1*/β-catenin. Immunofluorescence analysis of HCT116 β-catenin$^{wtClover/\Delta45}$ and β-catenin$^{wt/\Delta45Cherry}$ after siRNA-mediated knockdown of *CTNNB1* is shown (n=3; mean ± SEM; scale bar, 100µm). (B) β-catenin accumulates at cell-cell junctions (arrow). Representative immunofluorescence of HCT116 β-catenin$^{wtClover/\Delta45}$, β-catenin$^{wt/\Delta45Cherry}$ and parental HCT116$^{wt/\Delta45}$ stained with β-catenin antibody is shown. Scale bar = 10µm. (C) Immunoprecipitation of HCT116 β-catenin$^{wtClover/\Delta45}$ and β-catenin$^{wt/\Delta45Cherry}$ with E-cadherin validates its interaction with β-catenin. A representative immunoblot is displayed.

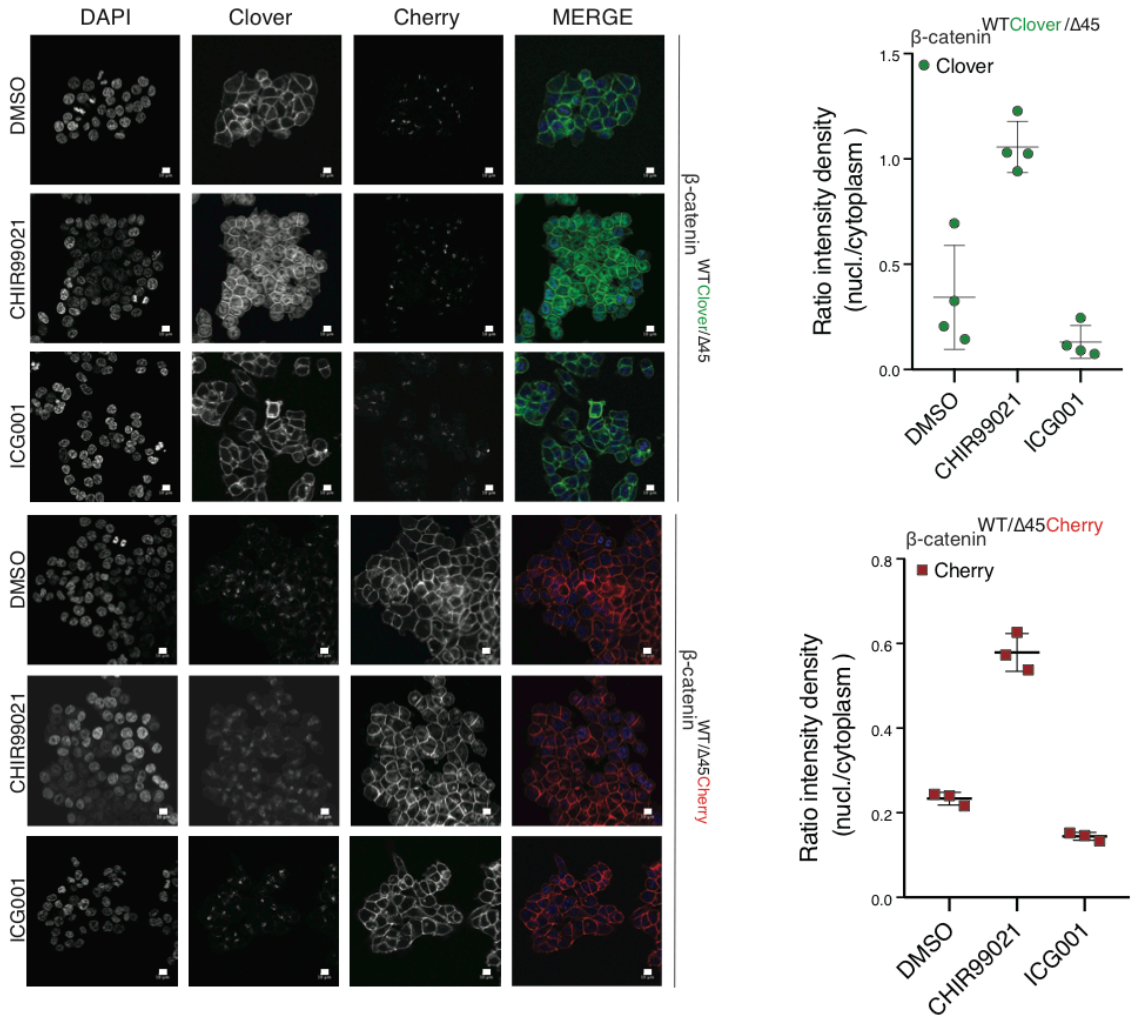

Figure S4: Tagging of β-catenin does not affect its functionality in canonical Wnt signaling. Immunofluorescence analysis of HCT116 β-catenin$^{wtClover/\Delta45}$ and β-catenin$^{wt/\Delta45Cherry}$ after 24 hours treatment with 10µM CHIR99021 and 10µM ICG-001 is shown. The graphs on the right show the ratio of nuclear to cytoplasmic fluorescence intensities for Clover and Cherry in β-catenin$^{wtClover/\Delta45}$ and β-catenin$^{wt/\Delta45Cherry}$, respectively (n=3 and4; mean ± SEM). Scale bar, 10µm.

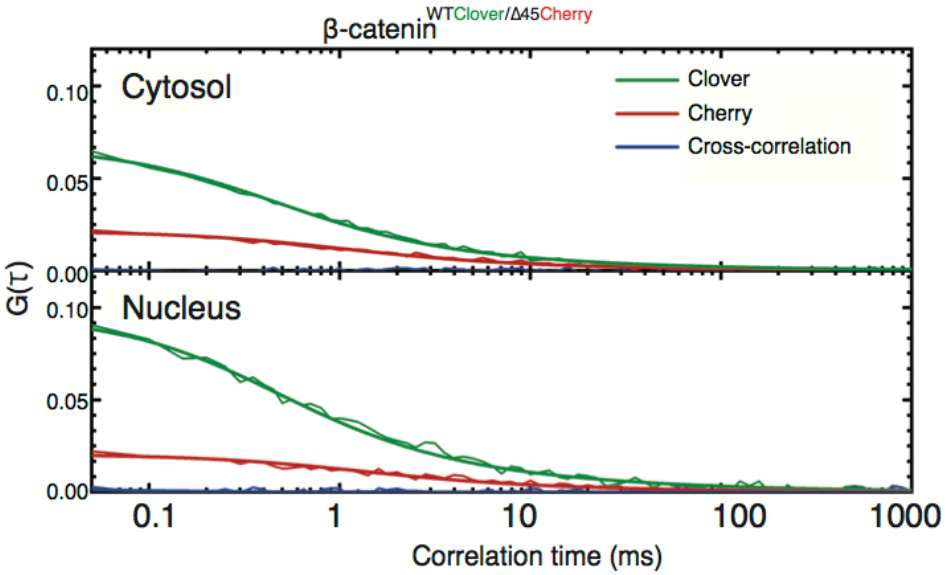

Figure S6: Cross-correlation analysis reveals that the two β-catenin protein isoforms diffuse independently. Shown are representative autocorrelation curves (green, red) and the cross-correlation (blue) from 120-s FCS measurements in the cytosol and the nucleus of HCT116 β-catenin$^{wtClover/\Delta45Cherry}$. The non-zero amplitudes of the autocorrelation curves in the green and red color channels indicate the presence of both β-catenin isoforms in the cytosol and in the nucleus. Jagged lines: experimental data, smooth lines, fits with a model function, y-axis: amplitudes of the pair correlation functions.

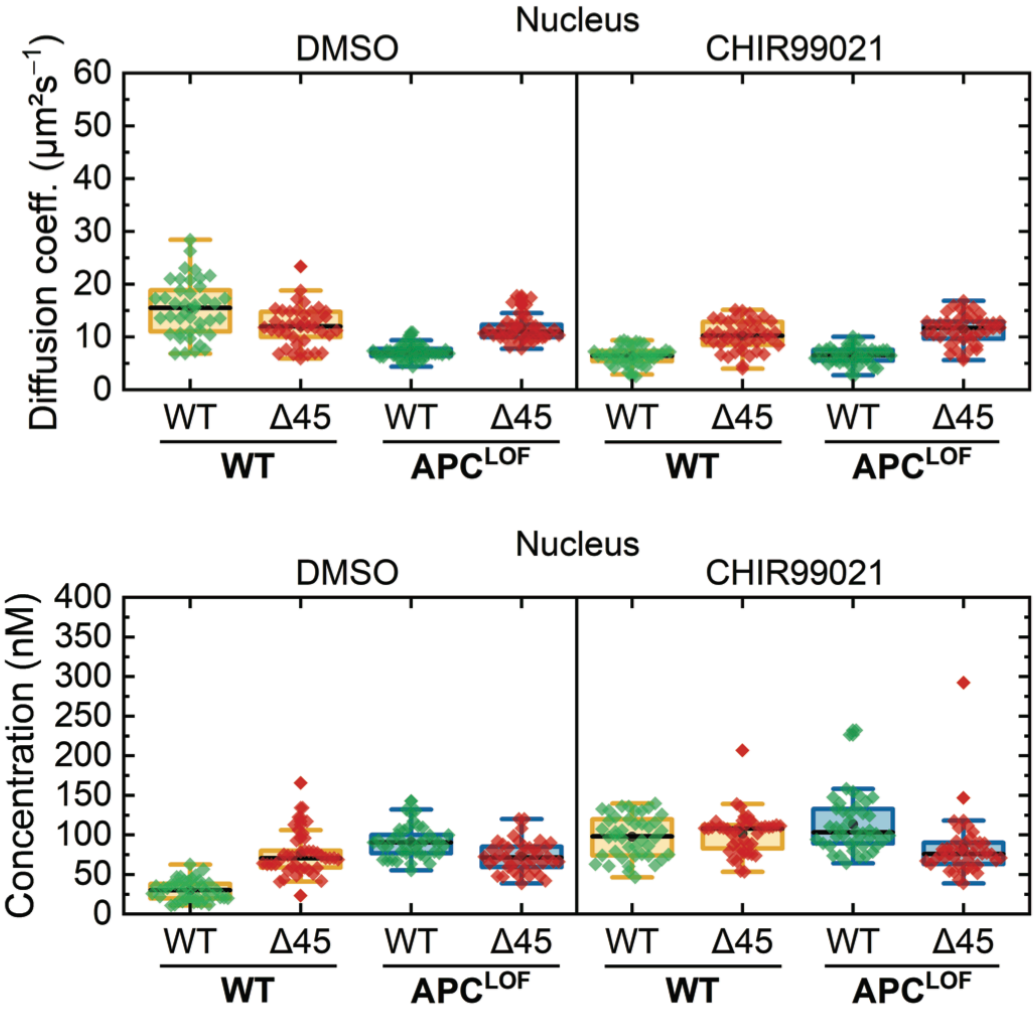

Figure S7: Truncation of APC affects abundance and diffusion of wild-type but not mutant β-catenin in the nucleus. HCT116 β-catenin$^{wtClover/\Delta45Cherry}$ and sgAPC targeted clone (APC^{LOF}) cells were treated for ~16 h with either 10 µM CHIR9901 or DMSO as control. Afterwards, FCS measurements were performed in the cytosol (data shown in Figure 7) and in the nucleus (shown here). For each data point, a 120-s FCS measurement was carried out in a single cell. Per box plot, more than 40 cells were examined in three independent experiments.

REFERENCES

Aberle, H., S. Butz, J. Stappert, H. Weissig, R. Kemler, and H. Hoschuetzky. 1994. Assembly of the cadherin-catenin complex in vitro with recombinant proteins. *J. Cell Sci.* 107 (Pt 12):3655–3663.

Bilic, J., Y.-L. Huang, G. Davidson, T. Zimmermann, C.-M. Cruciat, M. Bienz, and C. Niehrs. 2007. Wnt induces LRP6 signalosomes and promotes dishevelled-dependent LRP6 phosphorylation. *Science*. 316:1619–1622.

Cancer Genome Atlas Network. 2012. Comprehensive molecular characterization of human colon and rectal cancer. *Nature*. 487:330–337.

Carpenter, A.E., T.R. Jones, M.R. Lamprecht, C. Clarke, I.H. Kang, O. Friman, D.A. Guertin, J.H. Chang, R.A. Lindquist, J. Moffat, P. Golland, and D.M. Sabatini. 2006. CellProfiler: image analysis software for identifying and quantifying cell phenotypes. *Genome Biol.* 7:R100.

Chan, T.A., Z. Wang, L.H. Dang, B. Vogelstein, and K.W. Kinzler. 2002. Targeted inactivation of CTNNB1 reveals unexpected effects of beta-catenin mutation. *Proc. Natl. Acad. Sci. U. S. A.* 99:8265–8270.

Clevers, H., and R. Nusse. 2012. Wnt/β-catenin signaling and disease. *Cell*. 149:1192–1205.

Cliffe, A., F. Hamada, and M. Bienz. 2003. A role of Dishevelled in relocating Axin to the plasma membrane during wingless signaling. *Curr. Biol.* 13:960–966.

Cong, F., L. Schweizer, and H. Varmus. 2004. Wnt signals across the plasma membrane to activate the beta-catenin pathway by forming oligomers containing its receptors, Frizzled and LRP. *Development*. 131:5103–5115.

Cong, L., F.A. Ran, D. Cox, S. Lin, R. Barretto, N. Habib, P.D. Hsu, X. Wu, W. Jiang, L.A. Marraffini, and F. Zhang. 2013. Multiplex genome engineering using CRISPR/Cas systems. *Science*. 339:819–823.

Dambournet, D., S.H. Hong, A. Grassart, and D.G. Drubin. 2014. Tagging endogenous loci for live-cell fluorescence imaging and molecule counting using ZFNs, TALENs, and Cas9. *Methods Enzymol.* 546:139–160.

Dar, M.S., P. Singh, R.A. Mir, and M.J. Dar. 2017. Beta-catenin N-terminal domain: An enigmatic region prone to cancer causing mutations. *Mutat. Res.* 773:122–133.

Demir, K., N. Kirsch, C.A. Beretta, G. Erdmann, D. Ingelfinger, E. Moro, F. Argenton, M. Carl, C. Niehrs, and M. Boutros. 2013. RAB8B is required for activity and caveolar endocytosis of LRP6. *Cell Rep.* 4:1224–1234.

Dörlich, R.M., Q. Chen, P. Niklas Hedde, V. Schuster, M. Hippler, J. Wesslowski, G. Davidson, and G.U. Nienhaus. 2015. Dual-color dual-focus line-scanning FCS for quantitative analysis of receptor-ligand interactions in living specimens. *Sci. Rep.* 5:10149.

Eckert, A.F., P. Gao, J. Wesslowski, X. Wang, J. Rath, K. Nienhaus, G. Davidson, and G.U. Nienhaus. 2020. Measuring ligand-cell surface receptor affinities with axial line-scanning fluorescence correlation spectroscopy. *eLife*. 9. doi:10.7554/elife.55286.

Elliott, B., C. Richardson, J. Winderbaum, J.A. Nickoloff, and M. Jasin. 1998. Gene conversion tracts from double-strand break repair in mammalian cells. *Mol. Cell. Biol.* 18:93–101.

Fearnhead, N.S., M.P. Britton, and W.F. Bodmer. 2001. The ABC of APC. *Hum. Mol. Genet.* 10:721–733.

Foo, Y.H., V. Korzh, and T. Wohland. 2012. Fluorescence Correlation and Cross-Correlation Spectroscopy Using Fluorescent Proteins for Measurements of Biomolecular Processes in Living Organisms. *In* Fluorescent Proteins II: Application of Fluorescent Protein Technology. G. Jung, editor. Springer Berlin Heidelberg, Berlin, Heidelberg. 213–248.

Fuchs, F., G. Pau, D. Kranz, O. Sklyar, C. Budjan, S. Steinbrink, T. Horn, A. Pedal, W. Huber, and M. Boutros. 2010. Clustering phenotype populations by genome-wide RNAi and multiparametric imaging. *Mol. Syst. Biol.* 6:370.

Gao, P., B. Prunsche, L. Zhou, K. Nienhaus, and G.U. Nienhaus. 2017. Background suppression in fluorescence nanoscopy with stimulated emission double depletion. *Nat. Photonics*. 11:163–169.

Giannini, A.L., M.M. Vivanco, and R.M. Kypta. 2000. Analysis of beta-catenin aggregation and localization using GFP fusion proteins: nuclear import of alpha-catenin by the beta-catenin/Tcf complex. *Exp. Cell Res.* 255:207–220.

Goentoro, L., and M.W. Kirschner. 2009. Evidence that fold-change, and not absolute level, of beta-catenin dictates Wnt signaling. *Mol. Cell*. 36:872–884.

Gottardi, C.J., and B.M. Gumbiner. 2004. Distinct molecular forms of beta-catenin are targeted to adhesive or transcriptional complexes. *J. Cell Biol.* 167:339–349.

Hagen, T., and A. Vidal-Puig. 2002. Characterisation of the phosphorylation of beta-catenin at the GSK-3 priming site Ser45. *Biochem. Biophys. Res. Commun.* 294:324–328.

Heigwer, F., G. Kerr, and M. Boutros. 2014. E-CRISP: fast CRISPR target site identification. *Nat. Methods*. 11:122–123.

Hernández, A.R., A.M. Klein, and M.W. Kirschner. 2012. Kinetic responses of β-catenin specify the sites of Wnt control. *Science*. 338:1337–1340.

Hoadley, K.A., C. Yau, T. Hinoue, D.M. Wolf, A.J. Lazar, E. Drill, R. Shen, A.M. Taylor, A.D. Cherniack, V. Thorsson, R. Akbani, R. Bowlby, C.K. Wong, M. Wiznerowicz, F. Sanchez-Vega, A.G. Robertson, B.G. Schneider, M.S. Lawrence, H. Noushmehr, T.M. Malta, Cancer Genome Atlas Network, J.M. Stuart, C.C. Benz, and P.W. Laird. 2018. Cell-of-Origin Patterns Dominate the Molecular Classification of 10,000 Tumors from 33 Types of Cancer. *Cell*. 173:291–304.e6.

Hoschuetzky, H., H. Aberle, and R. Kemler. 1994. Beta-catenin mediates the interaction of the cadherin-catenin complex with epidermal growth factor receptor. *J. Cell Biol.* 127:1375–1380.

Huber, A.H., W.J. Nelson, and W.I. Weis. 1997. Three-dimensional structure of the armadillo repeat region of beta-catenin. *Cell*. 90:871–882.

Huber, A.H., and W.I. Weis. 2001. The structure of the beta-catenin/E-cadherin complex and the molecular basis of diverse ligand recognition by beta-catenin. *Cell*. 105:391–402.

Jamieson, C., M. Sharma, and B.R. Henderson. 2011. Regulation of β-catenin nuclear dynamics by GSK-3β involves a LEF-1 positive feedback loop. *Traffic*. 12:983–999.

Kafri, P., S.E. Hasenson, I. Kanter, J. Sheinberger, N. Kinor, S. Yunger, and Y. Shav-Tal. 2016. Quantifying β-catenin subcellular dynamics and cyclin D1 mRNA transcription during Wnt signaling in single living cells. *Elife*. 5. doi:10.7554/eLife.16748.

Krieghoff, E., J. Behrens, and B. Mayr. 2006. Nucleo-cytoplasmic distribution of beta-catenin is regulated by retention. *J. Cell Sci.* 119:1453–1463.

Lackner, D.H., A. Carré, P.M. Guzzardo, C. Banning, R. Mangena, T. Henley, S. Oberndorfer, B.V. Gapp, S.M.B. Nijman, T.R. Brummelkamp, and T. Bürckstümmer. 2015. A generic strategy for CRISPR-Cas9-mediated gene tagging. *Nat. Commun.* 6:10237.

Lam, A.J., F. St-Pierre, Y. Gong, J.D. Marshall, P.J. Cranfill, M.A. Baird, M.R. McKeown, J. Wiedenmann, M.W. Davidson, M.J. Schnitzer, R.Y. Tsien, and M.Z. Lin. 2012. Improving FRET dynamic range with bright green and red fluorescent proteins. *Nat. Methods*. 9:1005–1012.

Liu, C., Y. Li, M. Semenov, C. Han, G.H. Baeg, Y. Tan, Z. Zhang, X. Lin, and X. He. 2002. Control of beta-catenin phosphorylation/degradation by a dual-kinase mechanism. *Cell*. 108:837–847.

Li, V.S.W., S.S. Ng, P.J. Boersema, T.Y. Low, W.R. Karthaus, J.P. Gerlach, S. Mohammed, A.J.R. Heck, M.M. Maurice, T. Mahmoudi, and H. Clevers. 2012. Wnt signaling through inhibition of β-catenin degradation in an intact Axin1 complex. *Cell*. 149:1245–1256.

Mali, P., L. Yang, K.M. Esvelt, J. Aach, M. Guell, J.E. DiCarlo, J.E. Norville, and G.M. Church. 2013. RNA-guided human genome engineering via Cas9. *Science*. 339:823–826.

de Man, S.M.A., G. Zwanenburg, M.A. Hink, and R. van Amerongen. 2020. Quantitative live-cell imaging yields novel insight into endogenous WNT/CTNNB1 signaling dynamics. *Cell Biology*. 1619.

Martin, R.M., K. Ikeda, M.K. Cromer, N. Uchida, T. Nishimura, R. Romano, A.J. Tong, V.T. Lemgart, J. Camarena, M. Pavel-Dinu, C. Sindhu, V. Wiebking, S. Vaidyanathan, D.P. Dever, R.O. Bak, A. Laustsen, B.J. Lesch, M.R. Jakobsen, V. Sebastiano, H. Nakauchi, and M.H. Porteus. 2019. Highly Efficient and Marker-free Genome Editing of Human Pluripotent Stem Cells by CRISPR-Cas9 RNP and AAV6 Donor-Mediated Homologous Recombination. *Cell Stem Cell*. 24:821–828.e5.

Natsume, T., T. Kiyomitsu, Y. Saga, and M.T. Kanemaki. 2016. Rapid Protein Depletion in Human Cells by Auxin-Inducible Degron Tagging with Short Homology Donors. *Cell Rep.* 15:210–218.

Nickles, D., C. Falschlehner, M. Metzig, and M. Boutros. 2012. A genome-wide RNA interference screen identifies caspase 4 as a factor required for tumor necrosis factor alpha signaling. *Mol. Cell. Biol.* 32:3372–3381.

Orsulic, S., and M. Peifer. 1996. An in vivo structure-function study of armadillo, the beta-catenin homologue, reveals both separate and overlapping regions of the protein required for cell adhesion and for wingless signaling. *J. Cell Biol.* 134:1283–1300.

Pau, G., F. Fuchs, O. Sklyar, M. Boutros, and W. Huber. 2010. EBImage--an R package for image processing with applications to cellular phenotypes. *Bioinformatics*. 26:979–981.

Ran, F.A., P.D. Hsu, J. Wright, V. Agarwala, D.A. Scott, and F. Zhang. 2013. Genome engineering using the CRISPR-Cas9 system. *Nat. Protoc.* 8:2281–2308.

Rimm, D.L., E.R. Koslov, P. Kebriaei, C.D. Cianci, and J.S. Morrow. 1995. Alpha 1(E)-catenin is an actin-binding and -bundling protein mediating the attachment of F-actin to the membrane adhesion complex. *Proc. Natl. Acad. Sci. U. S. A.* 92:8813–8817.

Sahni, N., S. Yi, M. Taipale, J.I. Fuxman Bass, J. Coulombe-Huntington, F. Yang, J. Peng, J. Weile, G.I. Karras, Y. Wang, I.A. Kovács, A. Kamburov, I. Krykbaeva, M.H. Lam, G. Tucker, V. Khurana, A. Sharma, Y.-Y. Liu, N. Yachie, Q. Zhong, Y. Shen, A. Palagi, A. San-Miguel, C. Fan, D. Balcha, A. Dricot, D.M. Jordan, J.M. Walsh, A.A. Shah, X. Yang, A.K. Stoyanova, A. Leighton, M.A. Calderwood, Y. Jacob, M.E. Cusick, K. Salehi-Ashtiani, L.J. Whitesell, S. Sunyaev, B. Berger, A.-L. Barabási, B. Charloteaux, D.E. Hill, T. Hao, F.P. Roth, Y. Xia, A.J.M. Walhout, S. Lindquist, and M. Vidal. 2015. Widespread macromolecular interaction perturbations in human genetic disorders. *Cell*. 161:647–660.

Sanchez-Vega, F., M. Mina, J. Armenia, W.K. Chatila, A. Luna, K.C. La, S. Dimitriadoy, D.L. Liu, H.S. Kantheti, S. Saghafinia, D. Chakravarty, F. Daian, Q. Gao, M.H. Bailey, W.-W. Liang, S.M. Foltz, I. Shmulevich, L. Ding, Z. Heins, A. Ochoa, B. Gross, J. Gao, H. Zhang, R. Kundra, C. Kandoth, I. Bahceci, L. Dervishi, U. Dogrusoz, W. Zhou, H. Shen, P.W. Laird, G.P. Way, C.S. Greene, H. Liang, Y. Xiao, C. Wang, A. Iavarone, A.H. Berger, T.G. Bivona, A.J. Lazar, G.D. Hammer, T. Giordano, L.N. Kwong, G. McArthur, C. Huang, A.D. Tward, M.J. Frederick, F. McCormick, M. Meyerson, Cancer Genome Atlas Research Network, E.M. Van Allen, A.D. Cherniack, G. Ciriello, C. Sander, and N. Schultz. 2018. Oncogenic Signaling Pathways in The Cancer Genome Atlas. *Cell*. 173:321–337.e10.

Scholer-Dahirel, A., M.R. Schlabach, A. Loo, L. Bagdasarian, R. Meyer, R. Guo, S. Woolfenden, K.K. Yu, J. Markovits, K. Killary, D. Sonkin, Y.-M. Yao, M. Warmuth, W.R. Sellers, R. Schlegel, F. Stegmeier, R.E. Mosher, and M.E. McLaughlin. 2011. Maintenance of adenomatous polyposis coli (APC)-mutant colorectal cancer is dependent on Wnt/beta-catenin signaling. *Proc. Natl. Acad. Sci. U. S. A.* 108:17135–17140.

Schwarz-Romond, T., M. Fiedler, N. Shibata, P.J.G. Butler, A. Kikuchi, Y. Higuchi, and M. Bienz. 2007. The DIX domain of Dishevelled confers Wnt signaling by dynamic polymerization. *Nat. Struct. Mol. Biol.* 14:484–492.

Shaner, N.C., R.E. Campbell, P.A. Steinbach, B.N.G. Giepmans, A.E. Palmer, and R.Y. Tsien. 2004. Improved monomeric red, orange and yellow fluorescent proteins derived from Discosoma sp. red fluorescent protein. *Nat. Biotechnol.* 22:1567–1572.

Smirnikhina, S.A., A.A. Anuchina, and A.V. Lavrov. 2019. Ways of improving precise knock-in by genome-editing technologies. *Hum. Genet.* 138:1–19.

Stamos, J.L., M.L.-H. Chu, M.D. Enos, N. Shah, and W.I. Weis. 2014. Structural basis of GSK-3 inhibition by N-terminal phosphorylation and by the Wnt receptor LRP6. *Elife*. 3:e01998.

Thorn, K. 2017. Genetically encoded fluorescent tags. *Mol. Biol. Cell*. 28:848–857.

Trinh, R., B. Gurbaxani, S.L. Morrison, and M. Seyfzadeh. 2004. Optimization of codon pair use

within the (GGGGS)3 linker sequence results in enhanced protein expression. *Mol. Immunol.* 40:717–722.

Valenta, T., M. Gay, S. Steiner, K. Draganova, M. Zemke, R. Hoffmans, P. Cinelli, M. Aguet, L. Sommer, and K. Basler. 2011. Probing transcription-specific outputs of β-catenin in vivo. *Genes Dev.* 25:2631–2643.

Valenta, T., G. Hausmann, and K. Basler. 2012. The many faces and functions of β-catenin. *EMBO J.* 31:2714–2736.

Voloshanenko, O., G. Erdmann, T.D. Dubash, I. Augustin, M. Metzig, G. Moffa, C. Hundsrucker, G. Kerr, T. Sandmann, B. Anchang, K. Demir, C. Boehm, S. Leible, C.R. Ball, H. Glimm, R. Spang, and M. Boutros. 2013. Wnt secretion is required to maintain high levels of Wnt activity in colon cancer cells. *Nat. Commun.* 4:2610.

Wu, G., G. Xu, B.A. Schulman, P.D. Jeffrey, J.W. Harper, and N.P. Pavletich. 2003. Structure of a beta-TrCP1-Skp1-beta-catenin complex: destruction motif binding and lysine specificity of the SCF(beta-TrCP1) ubiquitin ligase. *Mol. Cell*. 11:1445–1456.

Xing, Y., K.-I. Takemaru, J. Liu, J.D. Berndt, J.J. Zheng, R.T. Moon, and W. Xu. 2008. Crystal structure of a full-length beta-catenin. *Structure*. 16:478–487.

Yang, L., J.L. Yang, S. Byrne, J. Pan, and G.M. Church. 2014. CRISPR/Cas9-Directed Genome Editing of Cultured Cells. *Curr. Protoc. Mol. Biol.* 107:31.1.1–17.

Zemanová, L., A. Schenk, M.J. Valler, G.U. Nienhaus, and R. Heilker. 2003. Confocal optics microscopy for biochemical and cellular high-throughput screening. *Drug Discov. Today*. 8:1085–1093.

Zhan, T., G. Ambrosi, A.M. Wandmacher, B. Rauscher, J. Betge, N. Rindtorff, R.S. Häussler, I. Hinsenkamp, L. Bamberg, B. Hessling, K. Müller-Decker, G. Erdmann, E. Burgermeister, M.P. Ebert, and M. Boutros. 2019. MEK inhibitors activate Wnt signalling and induce stem cell plasticity in colorectal cancer. *Nat. Commun.* 10:2197.

Zhan, T., N. Rindtorff, and M. Boutros. 2017. Wnt signaling in cancer. *Oncogene*. 36:1461–1473.

Zhong, Z., and D.M. Virshup. 2020. Wnt Signaling and Drug Resistance in Cancer. *Mol. Pharmacol.* 97:72–89.